Fracture peculiarities and high-temperature strength of bulk polycrystalline boron

D. Demirskyi (a,b,c)†, P. Badica (d)†, A. Kuncser (d), and O. Vasylkiv (c)†.

(a) WPI-Advanced Institute for Materials Research (WPI-AIMR), Tohoku University, 2-1-1 Katahira, Aoba-ku, Sendai, 980-8577 Japan.
(b) Department of Materials Science and Engineering, Tohoku University, 6-6-02 Aramaki Aza Aoba, Sendai, 980-8579, Japan.
(c) National Institute for Materials Science, 1-2-1 Sengen, Tsukuba, Ibaraki 305-0047, Japan.
(d) National Institute of Materials Physics, Street Atomistilor 405A, 077125, Magurele, Ilfov, Romania.

Abstract

We report the mechanical behavior of a bulk boron ceramic prepared by spark plasma sintering of commercially-available β-boron powder. In order to fabricate polycrystalline boron ceramic, we used a protective tantalum foil reacted with carbon from the graphite die or graphite foil forming a thin layer of TaB_2 and TaC covering the boron specimen. This is the first study to show the high-temperature flexural strength, toughness, and Young's moduli of boron up to 1400 °C. At 1600 °C and above, boron will react with testing environment forming an outer shell.

The flexural strength and fracture toughness at room temperature reached an average of 340 MPa and 4.1 MPa $m^{1/2}$, respectively. Despite showing clear signs of plastic deformation on the strain-stress curves, the yield strength of the monolithic boron ceramic exceed 1 GPa at 1200 °C. It was determined that fracture at elevated temperatures follows a quasi-transgranular mechanism, where the sub-grains of the boron fracture as plate-like structures. An interpretation for the observed fracture behavior was proposed.

Keywords: boron; polycrystalline ceramic; flexural strength; high-temperature materials.

1 Introduction

Boron is a unique ceramic which has a low specific density, high hardness, melting point above 2000 °C and high elastic properties at ambient temperature. This ensemble of physical and mechanical properties comes from the unique covalent bonding of boron [1,2]. Similar to carbon, boron has several allotropes, with α and β borons being the most common [3]. Due to these specific

† Authors to whom correspondence should be addressed, Dmytro Demirskyi, demirskyi.dmytro.e2@tohoku.ac.jp, Petre Badica petre.badica@infim.ro, Oleg Vasylkiv oleg.vasylkiv@nims.go.jp.

characteristics, boron is widely used in semiconducting electronics, rocket propellants, source for various borides, or as a material for shielding and neutron absorber in nuclear reactors [1,2].

Nevertheless, as for a typical ceramic, the brittle nature of bulk boron and the difficulty of preparing it have thus limited its use as a structural material. Besides, boron would react with almost any metal or non-metal at elevated temperatures [2], hence fabrication of high-purity monolithic boron is challenging. Although a large amount of work has been devoted to the amorphous form of boron or boron in the form of a fiber in the composite materials [4–6], only a limited number of studies have been directed towards the use of bulk crystalline boron as a structural ceramic [7–11]. Methods of preparation of fibers or filaments included processing of high-purity boron from boron chlorides with a maximum size of 20 μm [2]. Other methods, such as CVD [12], were used for ceramic coatings. Preparation of bulk monolithic boron is known to be achieved by melting in boron nitride crucible at 2050 °C [2]. Studies [7–11] are our source of information regarding the strength of polycrystalline boron, as values between 170 and 320 MPa were reported for the flexural strength at room temperature. Furthermore, various articles report that flexural and tensile tests of boron filaments exceeds 500 MPa [4–6], but no attempts were made to measure the elevated temperature fracture of bulk polycrystalline boron [7].

Within this study, we undertook the investigation of the flexural strength of bulk polycrystalline boron ceramic at elevated temperatures. One of the most challenging aspects was to fabricate high-purity polycrystalline boron ceramic. The bulk boron or boron powder will react with almost any substance at elevated temperatures. For this end, we used the spark plasma sintering method and used additional tantalum foil to minimize the carbon diffusion into the boron specimen during consolidation. The aim of this study was to define the extent of ductility for the polycrystalline boron, which was possible up to 1400 °C. Scanning and transmission electron microscopes were used to observe the structural changes during the consolidation and flexural tests. Finally, attempts were made to compare the fracture behavior of bulk polycrystalline boron ceramics with reports about boron carbide or boron suboxide bulks.

2 Materials and Methods

Commercially-available boron powder (Int Lab, USA, Lot#1012298) was used as the starting material. According to the manufacturer, the initial powder had a purity of >98% and powder particle size of 2 μm. Before consolidation, the boron powder with a red-rust color was diluted in

ethanol (C2H5OH, 99.5% reagent grade; Kanto Chemical Co.), stirred using a magnetic stirrer, then followed by low-temperature drying (at ~100 °C) to remove any moisture. The resultant powder was screened using a 60-mesh sieve.

The spark plasma sintering (SPS) experiments were conducted using the 'Dr. Sinter' 1050 (Sumitomo, Japan) unit with a 30-mm die. The schedule for the boron specimens prepared in this study had four major steps: (1) heating to 700 °C in four minutes following a five-minute dwell, (2) heating to 1000 °C in 10 minutes with a 10-minute dwell. After step (2), the heating rate of 50 °C min^{-1} was used to reach (3) the consolidation temperature of 1800 °C with a dwell of 15 minutes. The last step (4) was cooling to 600 °C in 15 minutes.

SPS was performed in a vacuum, as reports of the crystallization of amorphous boron [13,14] suggested that it will crystallize into the α-B form when argon is used, while processing in a vacuum favors crystallization of β-boron. At the end of the dwell at stage (2), the pressure was increased from 20 to 40 kN. The pressure of 40 kN was maintained during the consolidation and cooling stages. For simplicity, boron ceramic specimens prepared using the described procedure were labeled b15.

In order to minimize the reaction of boron with graphite foil or graphite punches/die during the spark plasma sintering, we used the tantalum foil (0.025-mm thick, 99.9+% metal basis; Sigma-Aldrich Japan G.K., Tokyo, Japan). The Ta foil was inserted between the powder and the graphite foil [15].

After consolidation, the surface of the sintered specimens had a gold-yellow or silver color. This was due to the formation of tantalum carbide or tantalum diboride, respectively. The layer consisting of these two phases extended up to 200 μm and was removed during polishing. Following removal of these layers, the surface of the boron ceramic had a dark grey color similar to that of boron carbide or boron suboxide. After coarse grinding, the sintered specimens were polished with diamond disks with a particle size of up to 0.5 μm. The density of the samples was then measured by the Archimedes method using ethanol as the medium in accordance with ASTM B 963–08.

An X-ray diffraction (XRD) analysis (D8 Advance, Bruker, Karlsruhe, Germany) using the Cu-Kα radiation was performed on the polished surfaces of the specimens. The intensity data were collected over the 2θ range of 20°–90°, in steps of 0.02°, using a sampling time of 2 s for each step. For the phase analysis, we used the range of 6°–46°, where data was collected in steps of

0.01° using a sampling time of 20 s for each step. The Ni filter was used to attenuate the Cu-Kβ radiation. The software used for the refinement was TOPAS (TOPAS Ver. 4.0, Bruker AXS, Germany) or MAUD. Instrumental broadening and specimen displacement was determined using a LaB_6 standard in runs under the same conditions for each boron sample. Lattice parameters of the boron ceramics were determined with an accuracy of 0.0001 Å.

Microstructural observations and analyses were carried out on the fracture surfaces by scanning electron microscopy (SEM, SU 8000; Hitachi, Tokyo, Japan) using a 5 kV acceleration voltage and secondary electrons mode. The details of the fine microstructure in boron ceramics after consolidation and after the flexural test at 1200 °C was observed by transmission electron microscopy (JEM 2100, TEM). TEM specimens were prepared by the standard powder method and plane-view method. For the plane-view method, mechanical polishing was followed by Ar-ion polishing using a Gatan PIPS (Precision Ion Polishing System). For simplicity, all the crystallographic indexes used in this study were in the (*hkl*) form calculated using the hexagonal (*hkil*) notation.

The three-point flexural strength was determined using rectangular blocks (2×2×25 mm or 1.5×2×25 mm) and strength testing equipment previously described in detail [16,17]. A span of 16 mm was used. Measurements were performed with a loading speed of 0.5 mm/min. Six to twelve samples were tested at room temperature from the ceramic tiles that were free of macroscopic cracks. The standard deviation was taken as the measurement accuracy. Tests above 1600 °C were performed in argon, otherwise, a vacuum atmosphere was used. In order to prevent reaction of the flexural bars made from boron with the B_4C-based loading cell, the surface of the bars was covered with a thin layer of hexagonal boron nitride as introduced in ref. [7]. The heating procedure for the high-temperature flexure tests was described in detail elsewhere [18].

The fracture toughness of the ceramics was evaluated using a specimen bending testing which contained a single edge through-thickness notch following ASTM C1421–10. Details of the testing configuration and the notch profile are presented in ref. [17]. Two tests with loading rates of 0.05 and 0.5 mm/min were performed at room temperature.

The hardness was determined by an MMT-7 Vickers hardness tester (Matsuzawa MMT-7; Matsuzawa SEIKI Co., Ltd., Tokyo, Japan) using a load of 9.8 N with a dwell time of 15 s following the standard procedure (ASTM C 1327–15).

3 Results and Discussion

3.1 Powder characterization

Figure 1 shows an SEM image of the initial powder and the results of the XRD analysis. The particles have an irregular shape and a size below 2 μm. The shape of the powders suggests that these were milled during the preparation. However, the absence of Fe (according to the EDX, Mg <500 ppm) suggests that after milling, the powder was chemically cleaned. The original powder had a dark red color which is consistent with previous studies [2,13]. One study [19] reported that the β-B powders had a star-like shape, which originated from the high-pressure synthesis [20]. Before the high-pressure synthesis, the amorphous boron powder used in [19,20] had a similar morphology to that in **Figure 1**.

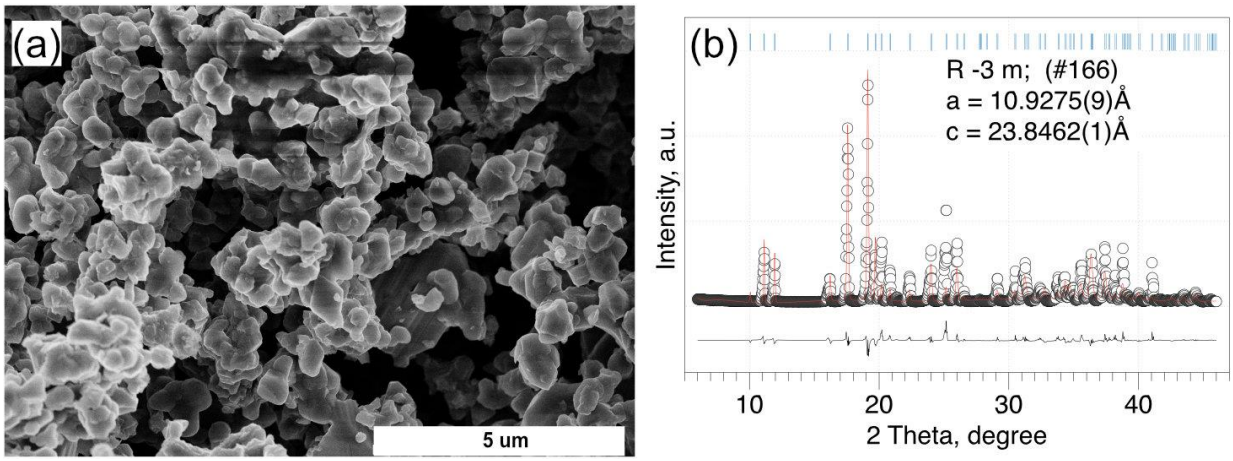

Figure 1. SEM and X-ray diffraction of the initial boron powder. All phases belong to the #166 (R-3m) space group. The main phase was β-B rhombohedral boron with the lattice parameters (a = 10.926 Å, c = 23.809 Å, [24,25]). The minor phase had lattice parameters second phase: a = 4.858 Å, c = 12.61 Å (2.85 vol.%) [23].

On the contrary, one work [21] suggested that both the color and powder shape (irregular or spherical) depend on the crystallinity of the powder. Nevertheless, the star-like shape is peculiar for the boron suboxide when the powder has been obtained by the chemical growth methods [21]. The XRD analysis and the color of the powder suggested a rather high-degree of crystallinity (70%) comparable to that observed for the boron powder in [21]. After sintering, the XRD showed that the rhombohedral β-B with the lattice parameters a = 10.926 Å, c = 23.809 Å remained as the main phase (98%). Only faint peaks were found and they can be attributed to the β-B with a high number of defects (a = 4.858 Å, c = 12.62 Å) [2].

Neither graphite or h-BN peaks were observed. But, secondary phases were detected in the samples. Because the impurity phase has a similar lattice parameter to that of the initial boron in the powder form, and also to $B_{13-x}N_2$ or $B_{13-y}O_2$ phases, based on the XRD results, it was not possible to identify the secondary phases. Boron carbides in any form were removed from the discussion considering the EDX results in SEM or TEM observation (see below) showing only traces of carbon in our samples. The lattice parameters for the secondary phase are slightly lower than that expected for boron suboxide (a = 5.3902 Å, c = 12.3125 Å) [22]. Following the analysis of [22], it can be expected that the lattice of the suboxide decreases with the oxygen occupancy of the *6c* site, suggesting that it is possible that the observed lattice parameters may indicate some local defects in O or N. We should emphasize that one study [23] reported the lattice parameter of the β-boron as a = 4.908 Å, c = 12.567 Å, which is comparable to the secondary phase obtained by XRD. The difference in volume of the cell for β-boron is due to a number of boron atoms considered for the hexagonal cell [23,24]. The main phase has a = 10.926 Å, c = 23.809 Å and this is consistent with the observation of Hoard for β-boron (a = 10.944 Å, c = 23.81 Å, or a = 10.145 Å and α = 65°17' rhombohedral lattice parameters) [24]. Hence, the data of ref. [24] were used in Rietveld refinement procedure.

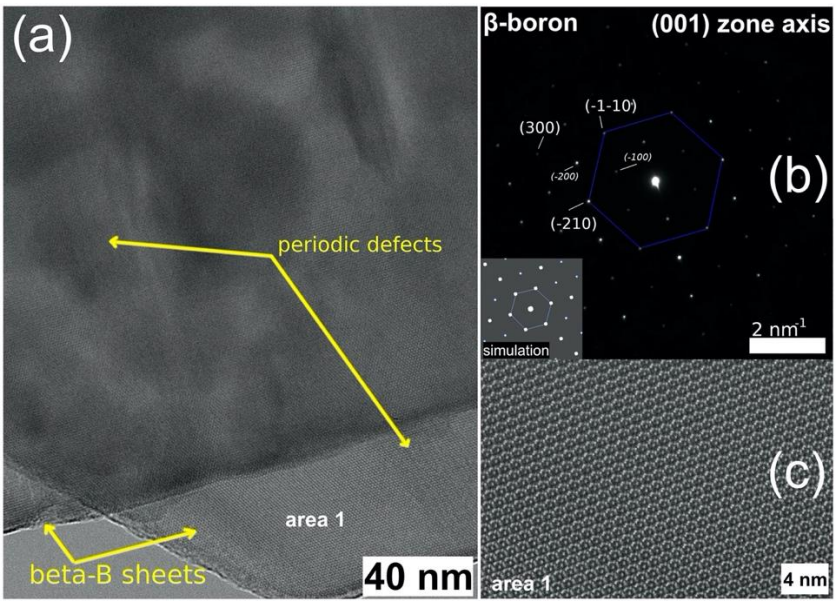

Figure 2. High-resolution TEM images of the as-received boron powder indicating that boron is composed of crystals with a layered aspect (a). SAED pattern in (b) indicates the β-B phase (cif data from ref [24]). The inset of the (b) shows a diffraction simulation under the kinematical theory assumption and is in good agreement with the experimental data. Some periodic defects can be

observed both within a single sheet and within a stacking of sheets. (c) shows the HRTEM details of a sheet as observed along the *c*-axis.

Figure 2 provides an indication of the local structure of the initial powder by high-resolution TEM. TEM images suggest that boron powder is composed of crystals with a layered nature. Periodic defects in the lattice were seldom. The SAED pattern in (**Figure 2 (b)**) is consistent with the initial XRD analysis as cif using the data of refs. [24] or [25] shows a good agreement between the experimental observation and diffraction simulation. The EDX analysis of the powder using TEM did not reveal metallic impurities in an amount higher than 500 ppm. These were Mg (~400 ppm), Al (~200 ppm) and Si (~100 ppm).

3.2 Densification

Before conducting the consolidation of boron using the schedule b15, various non-isothermal heating runs using SPS and a constant pressure of 40kN were performed. The densification behavior for the various process parameters is shown in **Figure 3**.

Studies on the obtaining or consolidation of bulk polycrystalline boron are few [8,9,26,27]. In [8], boron was prepared using chemical methods or by the arc-melting of the powder. The study [27] investigated the consolidation of boron at temperatures up to 2268K. In ref [27], a very coarse raw powder was used (8–10 μm) and thus a very low relative density can be understood from the Herring scaling law [28].

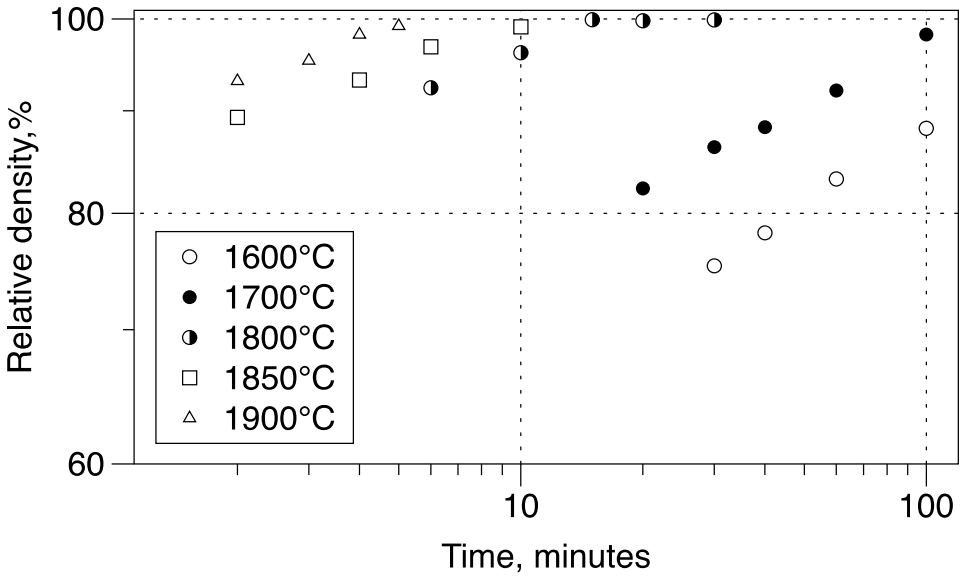

Figure 3. Isothermal densification of amorphous boron compacts using SPS.

A regular heating experiment using SPS suggested that the maximum shrinkage rate for the powdered β-Boron was at 1400 °C±80 °C, which is considerably less than observed in [27]. The consolidation in this temperature range using a dwell up to 30 min resulted in a poor density (below 70% TD). One of the factors in determining the final temperature for consolidation was to use a temperature range higher than for the dissociation of boron suboxide (>1760 °C) [29] in order to ensure that the resulting boron would be free from possible boron suboxide aggregates. Furthermore, because the tantalum foil was used during the SPS consolidation, the carbon diffusion was restricted to the surface layer of the boron specimens, where TaB_2 or TaC were formed and B_4C or $B_{13}C_2$ were not observed. As a rule, temperatures above 1850 °C resulted in coarse grain sizes (>5 μm) hence, the optimal temperature of 1800 °C was used.

The theoretical density of the b15 ceramic was evaluated as 2.425 g/cm^3, whereas the bulk density for the as-polished specimens was measured as 2.423 g/cm^3 (99.9 % TD). The mean grain size for the phases detected by SEM was below 2 μm (**Fig. 4**). The average grain size was 1.2±0.6 μm, while the median value of the grain size was estimated as 1.1 μm. The minimum grain size determined by SEM was 400 nm. The TEM results show the sizes of the grains/sub-grains below 500 nm.

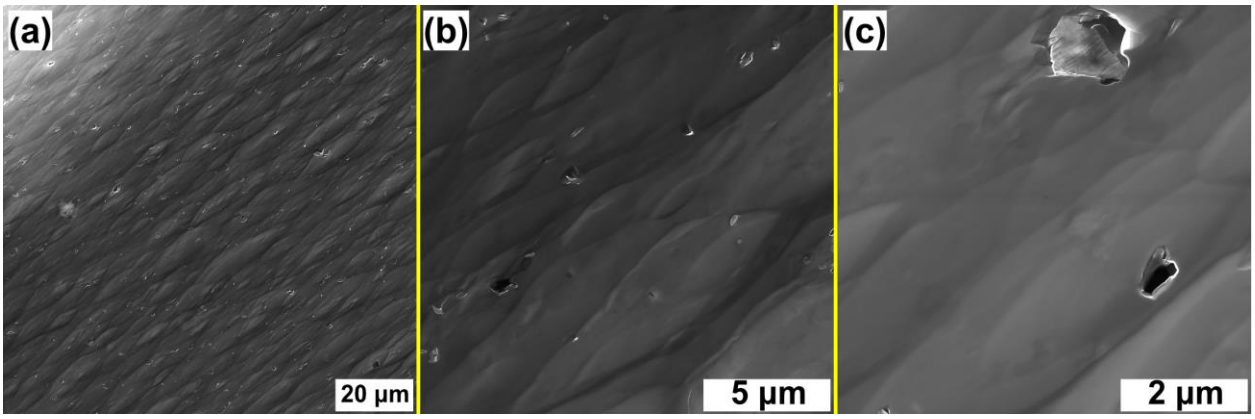

Figure 4. Representative microstructures of boron consolidated using SPS at 1800 °. Samples were prepared by ion polishing, as regular polishing using diamond slurry caused frequent pull-out of the 10–20 μm clusters.

3.3 Mechanical properties

The bulk b15 ceramic had a hardness of 32.1±0.6 GPa, which is comparable to monolithic boron carbide, boron suboxide or boron phosphides [2,30–33]. The toughness at ambient temperature did not exceed 4.1 MPa $m^{1/2}$, which is in agreement with the data for fine-grained boron carbide [33], boron suboxide [32] or boron phosphide [30].

The flexural strength test at room temperature showed that polycrystalline boron behaves in reasonable agreement with the strength vs grain size analysis for the boron-based ceramics presented in (**Figure 5**) [11,34–47]. The data are in close proximity to the results for monolithic boron suboxide [34] and boron – boron suboxide ceramics consolidated by Petrak et al. in [11]. That being said, the data for boron carbide presented in **Figure 5(a)** is quite broad as the majority of presented boron carbide bulks would have a minor amount (<1 vol%) of metallic or ceramic impurities, including graphitic carbon [48]. The data for b15 is marked with error bars, while the other bulk boron ceramics with slightly different grain sizes are summarized based on up to four flexural tests.

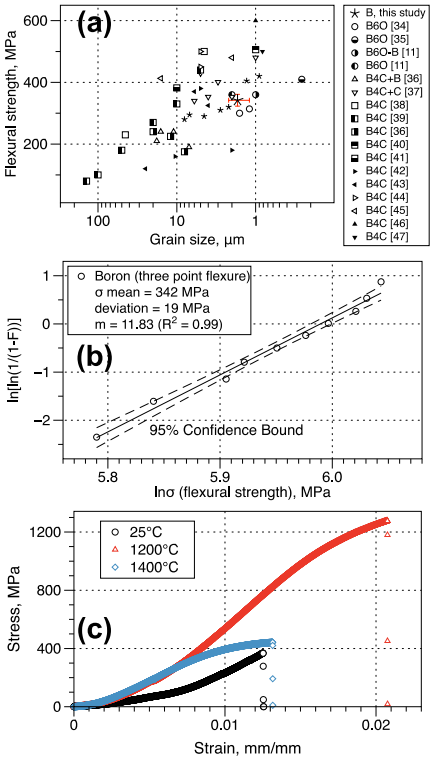

Figure 5. Flexural strength of boron ceramic: **(a)** variation in flexural strength of boron and boron carbide ceramics as a function of grain size [11,34–47]; **(b)** statistical variation in flexural strength at room temperature. **(c)** effect of temperature on the loading curves for bulk b15 ceramics at room temperature, at 1200 °C, and at 1400 °C.

The results of this study for the b15 ceramic (**Figure 5 (b)**) provide a very high Weibull factor, m = 11.83, which indicates that the majority of specimens would have similar in size strength–limiting flaws. This flaw should have a size of 20 or 32 μm depending on the flaw geometry using the Griffiths relation [49]. Judging from the average grain size for the b15 ceramic, this flaw should correspond to a surface flaw, as the flaw size only slightly exceeds a cluster consisting of ten boron grains. Since neither of the SEM images revealed grains with sizes larger than 8 μm, we consider the surface or subsurface flaw as the main candidate for the flaw that leads to fracture.

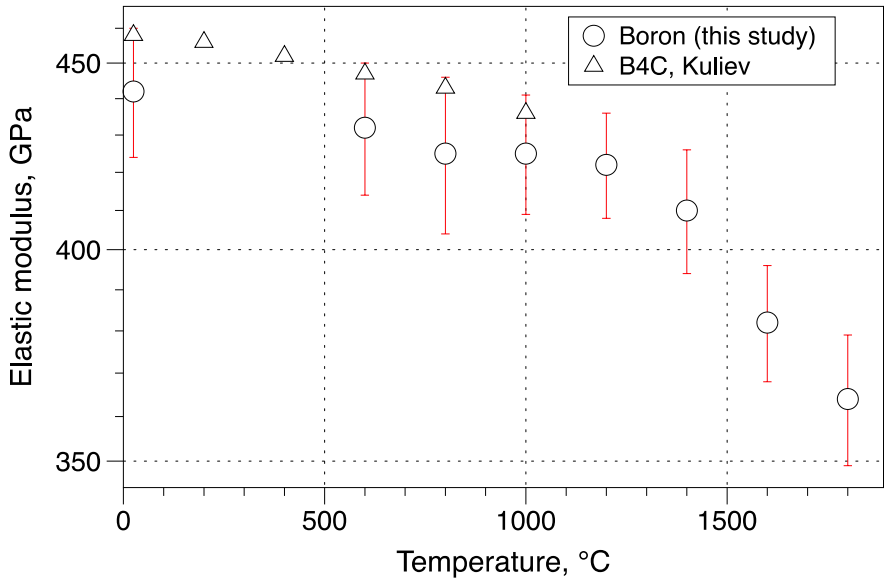

Figure 6. Young's modulus of bulk polycrystalline boron as a function of temperature. Data of Kuliev [51] for boron carbide is provided as a visual reference.

With an increase in temperature, the flaw size decreases below 6 μm (strength above 1100 MPa, toughness 3.3 MPa $m^{1/2}$, at 1200 °C), but in general, the fracture behavior is distinctively different than that observed at room temperature (see ***section 3.4***). We should note that 1200 °C was selected as roughly the 0.66 melting temperature of boron, as in this region for the metals and some covalent solids [50] plastic deformation should be a strength-controlling factor. Thus tests above this temperature as depicted in **Figure 5(c)** for 1400 °C would have a lower yield and fracture stress and will suffer from the of decrease Young's modulus (**Figure 6**) [51]. The variation of the fracture toughness vs temperature is summarized in **Figure 7**. The data for the high-temperature toughness dependence of the monolithic boron carbide, boron suboxide or boron ceramics were not available

at the time of this analysis. The data for B_6O–TaB_2 could not be directly compared [17] as TaB_2 may act as a toughening element. Without any reference data, it is impossible to analyze the observed temperature dependence of the toughness. We underline that the toughness gradually decreases with the increase in temperature and this decrease has striking similarities to the temperature dependence of the elastic modulus vs temperature (**Figure 6**). In this respect, it can be hypothesized that toughness at elevated temperature is not being improved by plasticity at the crack tip of the crack, and, in fact, the toughness decreases due to the decrease in the bonding between the grains.

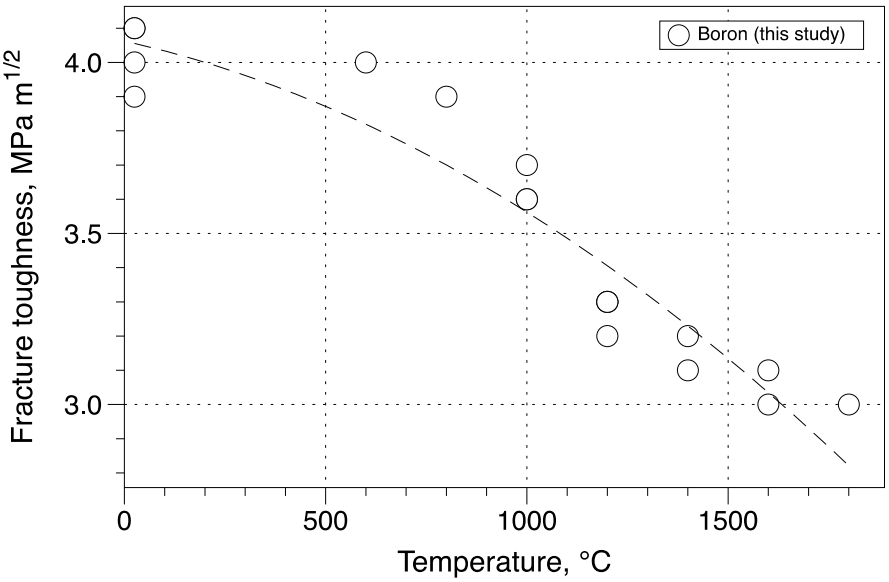

Figure 7. Fracture toughness of boron as a function of temperature.

The flexural strength data for boron [7], boron suboxide [34] and boron carbide [41,52,53] are summarized in **Figure 8**. In general, for the bulk boron carbide [54], various shapes of the strength vs temperature can be expected as such an increase in the strength observed for boron and for boron carbide [52,53] can be understood to be the consequence of the local increase in microplasticity [50]. Other factors, such as the local defect structure, obtained during processing (twins or stacking faults) may contribute to the strengthening. Another study [9,10] also reported the transverse rupture strength for boron samples with a high porosity (30%), and the strength for these specimens gradually decreased up to 1800 °C where plastic deformation was observed. The 1900 °C data in [9,10] yielded a four-fold decrease when compared to 1800 °C. This result can be interpreted as activation of the macroscopic plastic deformation of boron, and one can easily

understand why at temperatures between 1800 °C and 1900 °C densification was faster (**Figure 3**).

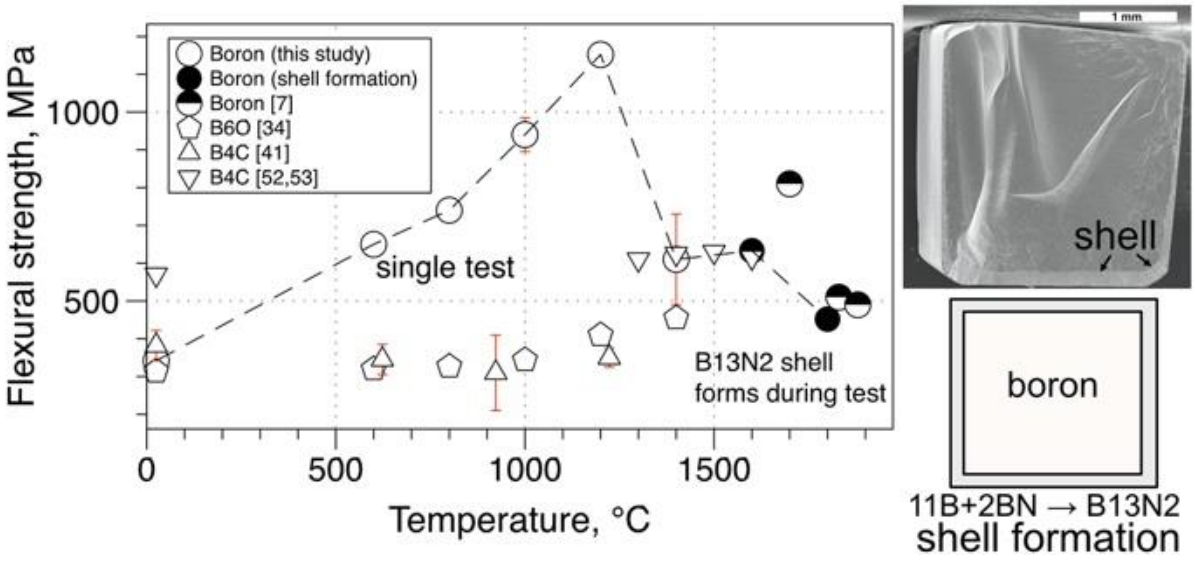

Figure 8. Summary of high-temperature flexure experiments for boron [7], boron carbide [41,52,53], and boron suboxide [34].

The rapid decrease in strength at 1400 °C could be interpreted as a higher contribution of plasticity to the fracture process, or alternatively (see ***section 3.4***), a change in the dominant fracture mode as result of, perhaps, activation of a different slip plane in the boron crystal. One may recall that for the flexural test we used BN powder to prevent a direct reaction between the boron specimens and boron carbide testing cells. Below 1600 °C, one could not observe any reaction between the boron and BN, while above this temperature, shells with a thickness between 100 and 200 μm were observed. The high reactivity of boron above 1500 °C is highly anticipated [2]. The data for the boron specimens tested at high temperatures of 1600 °C or 1800 °C depicted by the solid black circles in **Figure 8** are for specimens in which the formation of the outer shell was observed during the flexural tests. The presence of a shell did not allow one to consider these data as "pure" boron. The similarity to the high-temperature data of boron and boron carbide [52,53] suggests that the optimal conditions for the bulk boron ceramics may lie below 1200 °C, where it is less reactive and possesses a high strength, relatively high toughness and high elastic modulus.

3.4 Fracture analysis of the boron at room temperature and at elevated temperatures

The fractographic analysis at room temperature suggested that monolithic boron behaves similar to glass-like ceramics. Macroscopic examination of the flexural bars after testing at any temperature showed that the middle section of the bar was shattered into at least 16 pieces of various sizes with largest direction being approximately 0.8 mm. The difference between the tests at room and elevated temperatures was in the size distribution with larger pieces being observed for tests at 1200 °C or 1400 °C. After the tests at the higher temperatures, see inset in **Figure 8**, one can still observe four to five pieces after fracture, but formation of the outer shell during the flexural test did not allow us to consider fracture for these specimens in this section. A fairly large number of pieces after the flexural test may serve as indirect confirmation that the fracture process is due to independent flaws, but in general, this significantly complicated the fracture analysis. It should be thus noted that monolithic pieces with a clear profile were used for the fractographic analysis by SEM or served the origin for the TEM specimens.

For the test at room temperature, typical brittle fracture has been observed, and depending on the area of the surface bar after the flexural strength tests, one can find the presence of the clusters of the secondary phases (**Figure 9**). The total area that these phases occupied was approximated ~8%, which is in agreement with the XRD data (see **Figure 1**). In general, there was a slight change in the lattice parameter of the main phase for the bulk a = 10.941 Å, c = 23.864 Å. Bragg peaks of the second phase are not shown in **Figure 9 (d)** as only four peaks can be attributed to the second phase. The lattice parameters were refined as a = 4.857 Å, c = 12.610 Å, which are consistent with earlier observations for the powder. Bulk ceramics of the boron showed some texture and preferred orientation, and these could not be resolved as planes with a similar symmetry would show a different preferred orientation. Thus, the refinement of the b15 bulks was attempted without taking into account the texture models. We attempted to improve the refinement of the bulk boron by taking into account the possibility of layered boron grains which were seldomly observed after fracture. The summary of these efforts are provided in **Figure 9 (e)** using four layers along the c axis for the hexagonal representation of β-boron. The refinement was significantly improved although a peak intensity mismatch due to the above-mentioned texture was still present. **Figure 9 (f)** illustrates the 'composite' consisting of the boron-matrix and layered boron inclusions as interpreted by the XRD data. From the macroscopic viewpoint, this situation can be described as a salami-like structure. One can only presume that such layered structures can be interpreted as N-rich grains following the SEM or TEM analysis.

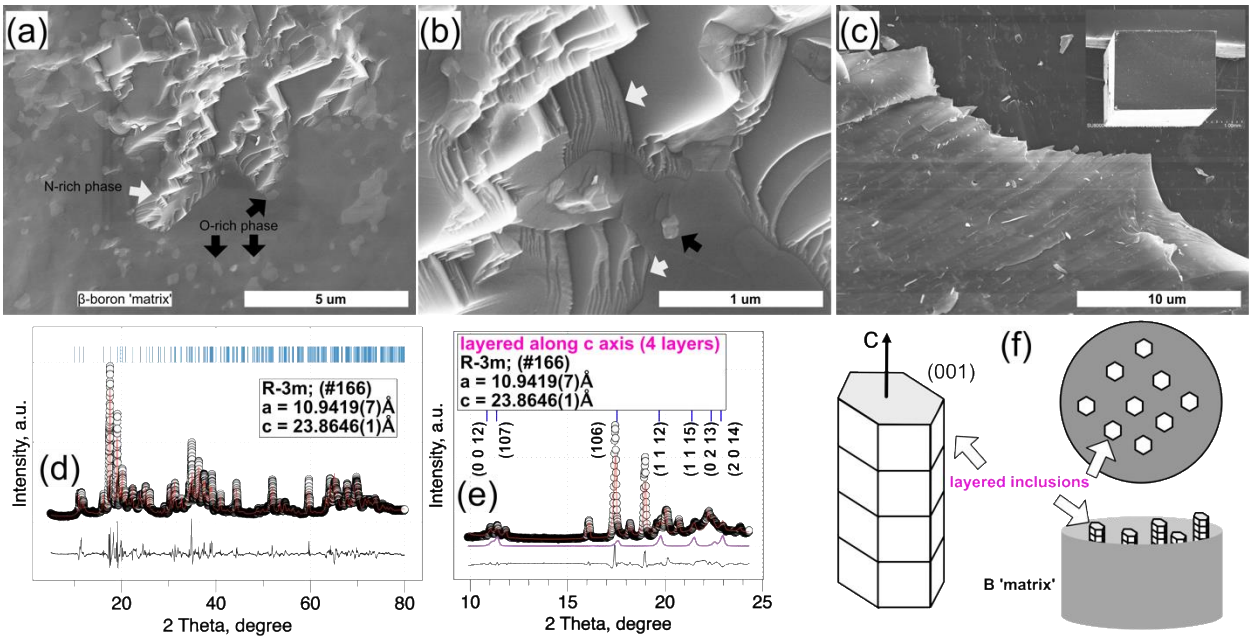

Figure 9. SEM images of b15 ceramics after flexural strength tests at room temperature. White arrows indicate N-rich grains, while black arrows indicate the presence of the O-rich precipitates. Based on the TEM observations, the size of the O-rich precipitates is approximately 50–200 nm, hence the light-gray grains that are larger in size correspond to the O-rich clusters. (c) shows a macroscopic zone where the B-matrix fractures in the intergranular manner and transgranular manner. The fracture type clearly depends on the relation to the force application. The O-rich precipitates are visible on both sides. Inset in (c) shows a macroscopic distribution of the large N-rich clusters and also illustrates the relation between the force application direction and fracture at room temperature. (d,e) shows a typical XRD pattern observed for the bulk b15 ceramic, and the blue lines indicate the Bragg position for the main phase using the same initial phase as for the powder material [24]. (e) highlighted position of peaks for the layered boron structures, while (f) provides a visual representation of the layered inclusions as seen by XRD. Such layered structures can be identified using the fracture as the N-rich phase. For these grains, multiple layers were observed following the flexural strength tests.

Furthermore, the fractured boron grains rich in N would spale in the layers or would lead to the formation of the triangle-shaped sharp-edge clusters. O-rich clusters usually remained embedded in the boron ‘matrix’, indicating that these may be precipitates formed during the SPS processing. The formation of edge-facets or (101) facets with a trigonal shape during the preparation of the

single-crystals of β-boron were observed in [55]. This was explained as specifics of the step-by-step growth or defect segregation in the form of the thermal etch pits. Hence, the presence of the minor phases that are rich in O or N can be understood to be a consequence of the SPS processing. As noted by Petrak et al. [11], the formation of the secondary phases in the bulk boron is unavoidable *per se* thus one can limit the amount of secondary phases when dealing, of course, with powder processing. In our case, as noted before, we restricted the diffusion of carbon to the surface of the specimens where it was consumed by the reaction between the carbon and tantalum foil formation TaC layer which was polished of after the SPS. If necessary, the formation of these clusters can be eliminated by SPS using lower temperatures. Other non-metal impurities, such as O or N, would arise, of course, from the direct exposure of the powder before the SPS. Although we did take precautions in using a glove box filled with argon during inserting the powder into the graphite die before the SPS. The short term exposure to moisture or air before the SPS processing was unavoidable within the present study.

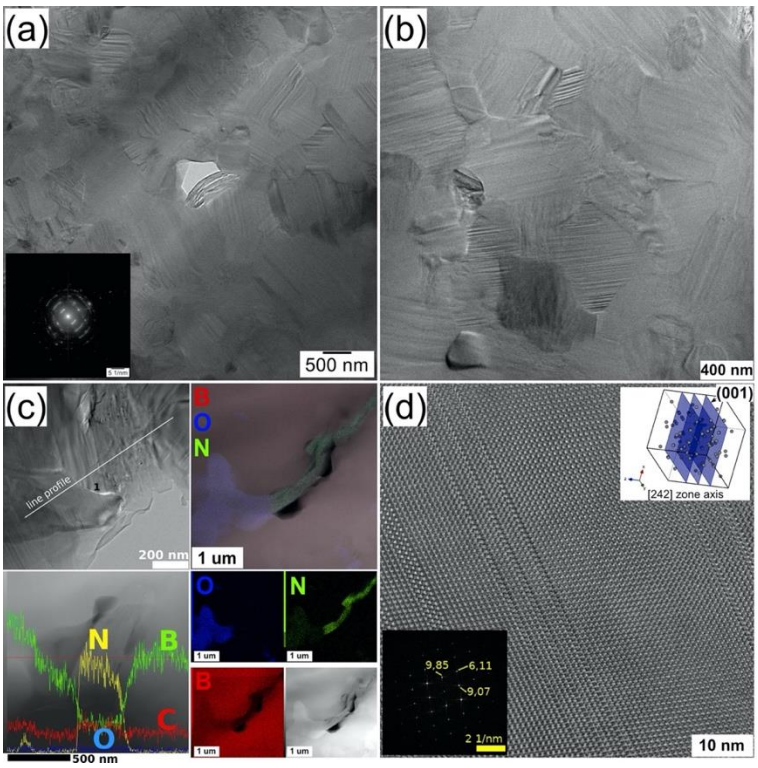

Figure 10. TEM images of b15 ceramics after (a) spark plasma consolidation at 1800 °C with 15-min dwell in argon and (b–d) following flexural strength tests at 1200 °C. Insets in (a, d) shows selected-area electron pattern of boron phases, identified as β-B (space group #166, using cif data from [24]). (d) shows local EDX mapping and line profile indicating the presence of the N-rich

and O-rich phases in the crystalline boron matrix. (d) shows a high resolution TEM image of a portion of an area marked as 1 in (c) in the [242] zone axis. 'Stacking faults' are visible here, but these were also present in the as-consolidated material (see grains in (a)). Inset in (d) visualizes (001) planes as possible stacking faults when 242 zone axis is used.

The TEM investigation of the boron bulk after consolidation or after the flexural tests at 1200 °C is summarized in **Figure 10**. One can see that the TEM images indicate that sub-grains with size of 400 nm were rather common after the consolidation or flexural tests. Only a fair amount of stacking faults as planar defects in these sub-grains occurred (**Fig. 10(b**)).

SAED patterns as in the case of the powder were analyzed by using the data of refs. [24, 25] converted into cif files from the NIMS database [56]. In general, the indicated cif files describe relatively well the structure as an average over a relatively large area (SAED inset in **Fig. 10 (a)** was taken on the entire area of **Fig. 10 (a**). However, the bulk boron samples locally contain nitrogen and oxygen as revealed by the EDS elemental line profiles and maps (**Fig. 10 (c)**). The maximum EDS measured stoichiometric ratios were B:O 100:3 and B:N 100:2.

The phase containing N was elongated (deformed and/or plate/rod-like), whereas the O-rich phase can be treated as a sub-grain or as a precipitate in the boron bulk and it has an irregular shape reminiscent of a frozen liquid. Some local regions, apparently when containing nitrogen and oxygen, show a higher presence of planar defects. Although their crystal structure resembles that for β-B it has different interplanar distances and lattice parameters (**Fig. 10 (d**)). We could not identify the phase in **Fig. 10 (d)** considering the known boron-like phases in the B-N and B-O systems and in the absence of reliable structural data for the phases of the B–C–N–O systems [57, 58] at the present moment, it was not possible to speculate on the formation of novel boron-rich phases.

However, a noteworthy observation concerns the presence of carbon in our samples. The TEM study indicated that C is present at the detection level. This suggested that application of tantalum foil is a reliable technique to minimize carbon diffusion into the pure polycrystalline boron material. The authors believe that suppression of the reaction between boron and carbon is important for successful fabrication of the boron polycrystalline bulks and may explain the current lack of reports on the fabrication of boron ceramics, but more research is needed to support this statement. An additional observation from the TEM investigations is that the oxygen-enriched

zones do not overlap with the zones rich in nitrogen. Under the presented circumstances, it is possible that for the unidentified structures of the oxygen and nitrogen-rich boron regions one has to consider other specifics of the boron. One idea is, as noted in ref. [59] for β-boron, that some of the B-sites, the B20 site in particular, would have a very low occupancy. Such sites are usually located close to the center of the hexagonal lattice (see **Figure 11**). At the same time, the authors of the ref. [59] suggested that the dominant impurity was carbon (150 ppm). However, the analysis in [59] suggested that 2 carbon atoms should be present in the 10 hexagonal unit cells of β-boron (each contains ~320 boron atoms). Hence, one may expect that oxygen and nitrogen can also provide a similar effect and further studies may clarify the existence of phases observed by the TEM or SEM.

The nitrogen-rich phases were seldomly observed as if formed by stackable layers and its fracture behavior was similar to that observed for the fracture of B_6O in [34] after flexural tests below 1000 °C. Phases rich in oxygen and nitrogen were clearly observed by the TEM during analysis of specimens after the flexural tests at room and at elevated temperatures.

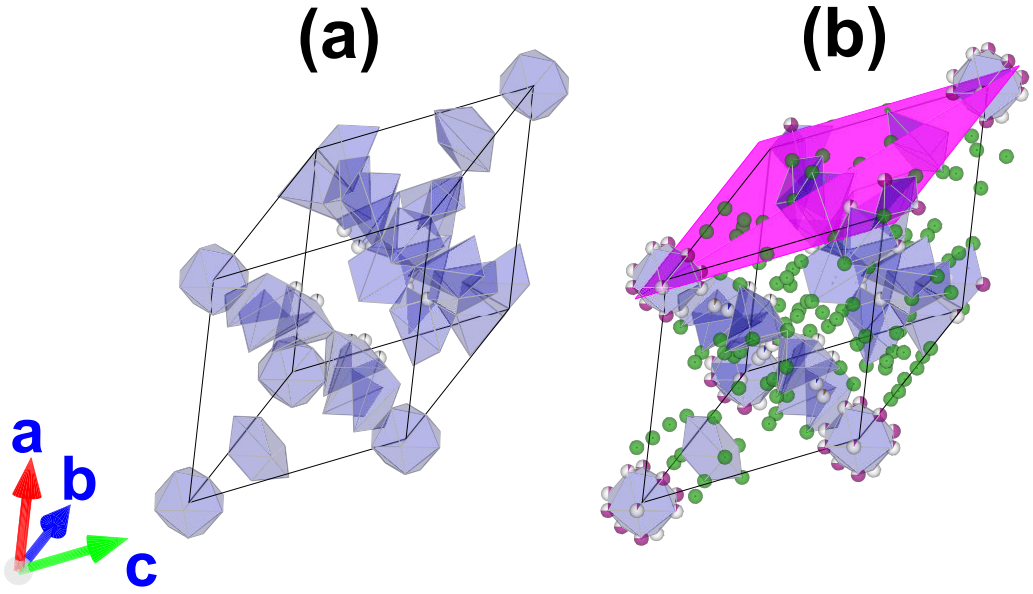

Figure 11. Position of B20 atoms with low partial occupancy in the β-boron according to structure refinement in [59]. (b) highlights the (100) plane for rhombohedral β-boron.

The B_6O phase is well known to have a non-stroichiometric composition with unoccupied sites in the center of the crystal [2] similar to the B20 position for β-boron. If so, this would support the idea presented in the previous paragraph. As consolidated b15 ceramic and the specimens after the

bending tests at 1200 °C showed the presence of multiple stacking faults (**Fig. 10 (b)**). Observation in the high-resolution TEM mode indicated that after deformation (**Fig. 10 (d)**) these areas consisted of lamellae boron layers between larger in size pairs of the stacking faults. Following a recent report on twins behavior in the boron carbide-based ceramic from ref. [54], it is suggested that the observed lamellae structures should correspond or be involved in the processes for twin formation, twin rearrangement and twin growth. In the scope of this study, the areas corresponding to twins were not identified by the TEM. Other studies [2,60] that could not identify twins have been reported for melted boron after high-temperature deformation [2, 60], although in some cases, stacking faults were observed. Based on **Fig. 10 (d)**, we may presume that stacking faults were observed parallel to the (001) plane.

3.4.1 Data on defects in bulk boron

Defects such as stacking faults, dislocations, and twins were reported in [2,55,60–66]. However, none of these studies were using polycrystalline boron prepared using powder metallurgy methods. In [2], it has been mentioned that dislocations could not be observed after high-temperature deformation of the crystals grown by the zone melting method, while the initial material had a considerable amount of stacking faults and twins, similar to the observations of [55] that were a consequence of the growth patterns. Analysis of the twins and dislocations by Werheit [61] indicated that a high concentration of structural defects in boron after melting may suggest that β-boron has a low energy for dislocation. Although some studies [60–62] mentioned observation of dislocations for melted boron, they failed to provide any crystallographic details.

Stacking faults in boron were reported in [61,63,64]. According to Kleinhenz and Runow [64] stacking faults for β-boron are situated in the (10-1) plane. Details on twins in α-boron [65,66] or β-boron [2,60,62,64] are more diverse. Ref. [65] reports that twining in α-boron obtained by pyrolysis in a hydrogen flaw was (100). Sitarik and Ellis [66] produced α-boron by the reduction of BCl_3 with hydrogen for transport and platinum as the liquid- forming agent. Both straight and kinked whisker crystals were produced with <-4401> growth directions. The twinning plane was (0 -1 14) for the rhombohedral crystal. For the β-boron, twinning plane of (5-1-1) in the hexagonal system is mentioned in [2], while [60,63,64] report (100) for the rhombohedral crystal (**Fig. 11 (b)**). At the same time ref [60] reported a possible twinning plane of (201), and it was underlined

that the calculation of defects using the plane (10-1) [64] was possible, however, such actions were insufficient to verify possible dislocation configuration.

These observations show that the polycrystalline boron situation with local defects are *even* more complex. Unlike observations made for specimens prepared by melting (arc-melting, zone melting, directional solidification, etc.) where the possibility exists to control the growth of crystals [2], specimens obtained by the 'powder metallurgy' approach should have a completely random pathway for the formation of grains from powders. The application of pressure during the SPS processing may serve as the parameter to alter the crystallization direction, as the boron powder crystalizes into α-B form or β-boron during heat-treatment [13,14]. Hence, fracture toughness and strength specimens were cut parallel to the pressure application direction, minimizing possible anisotropy in the measurements [2,55,60]. Thus, it is worthy to mention the results of Komatsu and Moriyoshi [67] which mention that β-boron may growth along quite different preferential directions including those that are not common for the above mentioned defects such as twins or stacking faults. Thus, the observed stacking faults (see **Fig. 10 (d)**) formed by a family of (001) planes may deviate from the (10-1) direction reported in [64].

3.4.2 Macroscopic fracture of bulk boron

Macroscopic fracture of boron bulks was analyzed by SEM. **Figure 12** summarizes the fractographic analysis performed after the flexural strength tests at elevated temperatures. Unlike fracture at room temperature, at 1200 °C, the b15 ceramic showed a more complex behavior. None of the fractured areas would follow classical intergranular or transgranular fracture mechanisms. Similar to observation in [67], the boron grains seem to fracture along a specific crystal orientation. From the view point of macroscopic fracture, the b15 ceramics showed characteristics of single-crystal sapphire or polycrystalline boron suboxide. Namely, in some instances as marked by the white arrows in **Figure 12**, the fractured areas would feature conchoidal surfaces. Based on previous studies of sapphire or corundum [68–71], it is most likely that these areas would correspond to the (012) plane (or to equivalent planes (-102), (1-12)). A similar formation has been observed for polycrystalline boron suboxide in [31], as grain surfaces were explored in the intermediate stages of the B_6O consolidation. With an increase in the testing temperature the volume fraction of the grains/clusters that are being fractured along the high-temperature slip-system increases from 68% for 1200 °C to 90% for 1400 °C. That being said, both quantitative

relationships between these two extreme cases are quite sensitive to the direction of the load application (see **Figures 12**). At temperatures above 1600 °C, 98% of the grains fracture in the manner presented in **Fig. 12 (f)**.

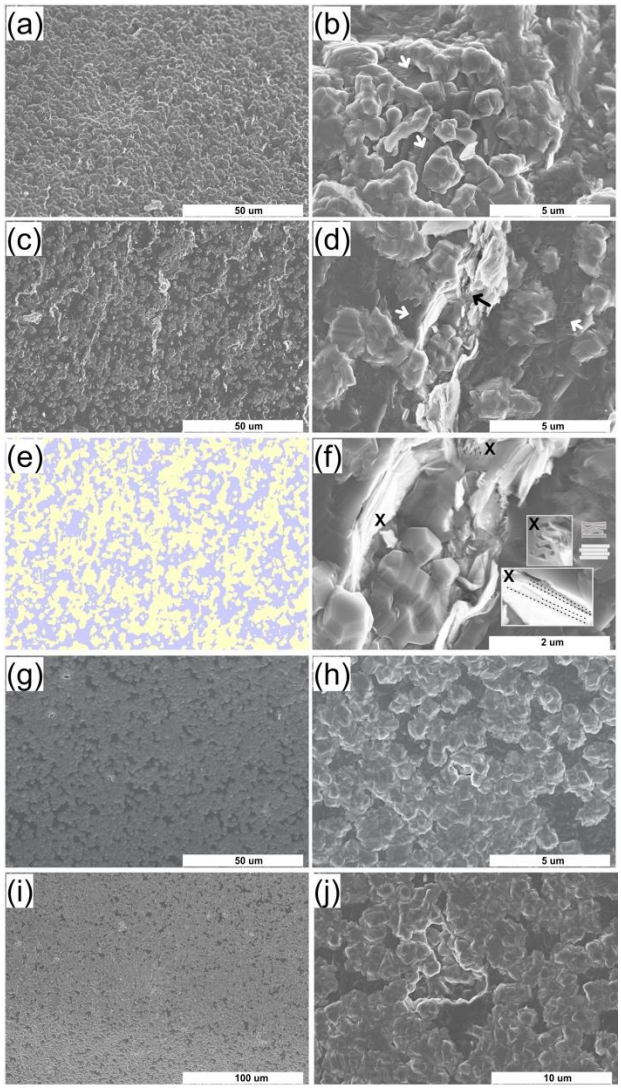

Figure 12. SEM micrographs of boron-15 after flexural tests at ambient temperature (a-d), at 1200 °C, and at 1400 °C (e,f). (a,b) were taken in the area at the ~40° angle to the load application direction, while (c-f) were taken from the surface perpendicular to the load application direction (top to bottom). The white arrows in (b,d) show places of quasi-brittle fracture previously reported for boron suboxide [31,34], and are the result of the fracture along (012) rhombohedral plane. The black arrow in (f) shows high-temperature plastic (rubberlike) deformation of layered boron grains (see higher magnification in (h)). (g) shows oversimplified view of (e) underlining the continuous nature of the matrix (blue (32 vol.%)) and suggesting that 2/3 of the grains fractured alongside the

low-temperature mechanism (see **Figure 14(c**)), while with an increase in temperature to 1400 °C, this value decreases below 10 vol% as the high-temperature slip-system should be dominant.

Our attempt to describe the high-temperature fracture process is presented in **Figures 13** and **14.** Some of the features observed in **Figs. 12–14** were previously observed during flexural tests of polycrystalline boron suboxide in [31]. Namely, plane-edge fracture with a pentagonal or pseudo-tetragonal prism shape. These could be understood if one revises the growth methods for some rhombohedral or hexagonal crystals (see inset in **Figure 13 (c)**). Thus, in the majority of fractured areas, the basal plane would be parallel to the loading direction, other grains should fracture alongside the high-temperature slip-system, and the (0-21)<110> is provided as an example in **Figure 14 (d)**. Here, the high-temperature fracture model for various slip-systems has been adapted from ref. [71], where the change in the active slip system was observed at elevated temperatures.

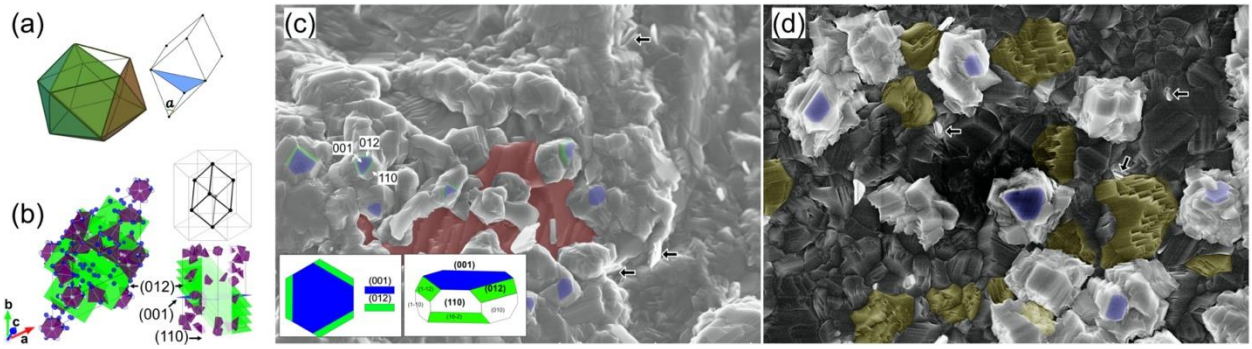

Figure 13. SEM images of b15 ceramics after flexural strength tests at 1200 °C. (a) shows an icosahedron which consists of 20 individual tetrahedral (which is the structure commonly observed for boron suboxide after high-pressure synthesis); right image illustrates relationship between icosahedron and rhombohedral cell. (b) shows the relationship of the rhombohedral cell of β-B and its hexagonal representation. The green plane selected in the β-B cell is (012) using the hexagonal indexes; the rhombohedral sapphire experiences conchoidal surfaces when fractured along this plane [68–71]. (c) Shows the (012) plane for the **Figure 12 (b)**, where the formation of conchoidal surfaces is highlighted in red. The blue highlights the typical fracture along the prismatic plane (presumably (100)). Formation of the pentagonal-shaped structures was also seldomly observed along the icosahedron faces. Inset in (c) provides an oversimplified illustration for the relation between the basal plane (001) and (012) lamellae form during growth of the rhombohedral crystals. The black arrows in (c) and (d) indicate the presence of nitrogen-rich phases.

Considering the results of refs. [67] or [72], one can expect that the amorphous phase can be crystallized in various directions. A change in the habitus growth direction is not a new phenomenon [73] and as covalent crystals, such as diamond, are also quite sensitive to impurities and external processing conditions. For instance, the development of the crystalline faces for the boron crystal presented as inset in **Figure 13 (c)** suggests that the (001) plane would most likely be the plane responsible for 'crystallization' of the boron from powder into the grains during the SPS. As for a brittle ceramics, the fracture of polycrystalline boron on the macroscopic level will be controlled by the low-temperature slip system, as the (001) plane may be responsible for growth of the crystals [2].

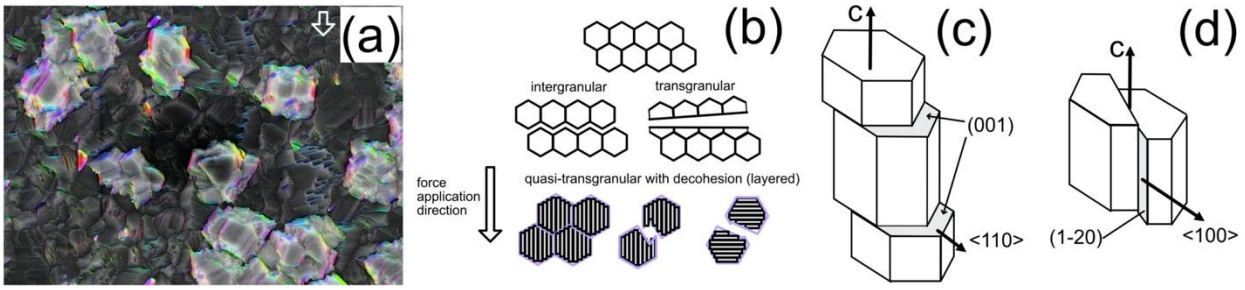

Figure 14. SEM images of b15 ceramics after flexural strength tests at 1200 °C, where the white arrows shows orientation of boron grains with the respect to the force application direction. Similar fracture has been reported for boron suboxide below 1000 °C in [34] and after consolidation in [31]. In principle, if grains consist of layered sub-grains, this fracture mechanism should not be limited to boron-rich compounds. (b) depicts a nominal fracture mechanism of quasi-transgranular fracture, as decohesion is assumed to be active for a boron ceramic at elevated temperatures. Directions for fracture in (a) were determined by OrientationJ (ImageJ), and note that the conchoidal surfaces usually form along the (012) plane. (c and d) provide a schematic comparison of two slip systems previously observed by Scheuplein [71]. (c) is typical for low temperature deformation, while (d) corresponds to the high-temperature slip system.

By comparing the TEM and SEM results, it can be suggested that because the fracture macroscopically occurs mainly by peculiar slip systems, only the zone affected by the high-temperature crack propagation would reveal fracture mechanisms. SEM studies suggested that it was not possible to identify the oxygen-rich grains for specimens tested at elevated temperatures, while stackable small sized structures similar to that for the nitrogen-enriched areas were seldomly

identified (black arrows in **Figures 12, 13**). In contrast both phases were identified by TEM after tests at elevated temperatures. We attempted the flexural tests in a vacuum, nitrogen and argon at 1200 °C, and the testing atmosphere did not affect the macroscopic fracture behavior or changes in the XRD profiles. Thus, it can be assumed that the phases identified by TEM as nitrogen and oxygen enriched grains belong to a solution of these atoms in the boron crystal rather than novel compounds. It is known that the beta boron lattice can form a solid-solution with a number of metals without altering the β-boron lattice packing. In this case, up to 5 mol.% metal can be distributed in the lattice, and the volume of the lattice cell increases up to 4 % [74].

For the stochiometric boron suboxide, for instance, the oxygen deficiency for the *6c* position would lead to the decrease in volume of the cell, but as already discussed, the presence of non-metal atoms in the highly ordered boron cell causes the difference in lattice parameters between β-boron and $B_6O_{0.95}$ (in hexagonal axis: β-B a = 10.932 Å, c = 23.823 Å, $B_6O_{0.95}$ a = 5.390 Å, c = 12.312 Å), but one should keep in mind that the electroneutrality of the crystal should be preserved. One can presume that the observed B–N or B–O phases can be localized solid-solution by substitution mechanisms, but in the absence of previous reports predicting [57,58] such a situation, we are unable to come to justifiable conclusions on this matter.

From a practical point of view, boron ceramics can be proposed as a reinforcement for the composites with a temperature application below 1200 °C (the estimated Young's moduli from linear parts of the loading curves was 410 GPa). This is similar to the well-known application for the boron as filaments or whiskers [2]. As a stand-alone ceramic boron would react with graphite during the SPS or boron-carbide testing assembly above 1000 °C, this causes a need for the development of protection. Note that the elevated temperature strength as well as fracture behavior for the boron ceramic prepared within the present study is different. Considering the flexural strength values, the yield strength for the specimen tested at 1000 °C which is above 800 MPa, is superior to monolithic boron carbides that have a maximum reported strength of ~600 MPa at elevated temperatures [52,53]. Flexural strength at 1200 °C exceeding 1 GPa was measured, but above this temperature the plastic deformation was present for all specimens.

Summary

This is a pioneering study that reports the mechanical behavior of bulk polycrystalline boron. The preparation and mechanical behavior of the bulk boron ceramic were discussed with respect to the

spark plasma sintering and high-temperature fracture mechanisms. Our results show confirm that polycrystalline boron is highly reactive ceramic and will react with BN or B_4C at temperatures above 1600 °C. During flexural tests this will result in formation of the outer shell consisting of $B_{13}C_2$ or $B_{13}N_2$.

Thus the high-temperature performance of monolithic boron can be analyzed up to 1400 °C. With an increase in the temperature, both the toughness and Young's moduli showed a gradual decrease. Flexural strength increased up to 1200 °C (yield strength above 1 GPa) and then decreased to ~600 MPa at 1400 °C. The rapid decrease in strength at 1400 °C could be interpreted as a higher contribution of plasticity to the fracture process. Furthermore, formation of the pentagonal-shaped structures was also observed during the fracture analysis. For this reason, relation between the basal plane (001) and the (012) plane becomes clear at 1200 °C. It was determined that the fracture above 1200°C follows a quasi-transgranular mechanism, where the sub-grains of boron fracture as plate-like structures following a combination of low-temperature and high-temperature slip systems.

Acknowledgements

Authors express their sincere appreciation to Dr. Toshiyuki Nishimura (NIMS) for providing access to the evaluation of high-temperature strength. D.D. was supported by World Premier International Research Center Initiative (WPI), MEXT, Japan. PB and AK acknowledge support from UEFISCDI Romania through Core Program PN19-03 (contract no. 21 N/08.02.2019) and projects 74-COFUND-M-ERA.NET II—BIOMB, 5PTE/2020—BIOTEHKER.

Compliance with Ethical Standards

The authors declare that they have no conflict of interest.

References

[1] V.I. Matkovich (ed).: Boron and refractory borides. Springer-Verlag: Berlin, Heidelberg, New York, 1977.

[2] G.V. Tsagareishvili, F.N. Tavadze. Semiconductor boron. Nauka: Moscow, 1978. [in Russian].

[3] J.L Hoard, Remarks on structure and polymorphism in boron, in: Kohn J.A., Nye W.F., Gaulé G.K. (eds.) Boron Synthesis, Structure, and Properties. Springer: Boston, MA, 1960.

[4] F.E. Wawner, The Effect of Chemical Polishing on the Strength and Fracture Characteristics of Amorphous Boron Filaments. In: Gaulé G.K. (eds) Boron. Springer: Boston, 1965.

[5] R. Veltri, F. Galasso, Tensile Strength of Boron Filament coated with Silicon Carbide and of Uncoated Boron Filament at Elevated Temperatures, Nature 220 (1968) 781–782.

[6] R.T. Schwartz, H.S. Schwartz, Characteristics of boron fibers and boron- fiber-reinforced plastic composites, AIAA Journal 5 [2] (1967) 289–295.

[7] G.V. Tsagareishvili, A.G. Khvadelidze, G.V. Berezhkova, G.V. Govorkov, N.N. Voinova, Some mechanical properties β-rhombohedral boron crystals. In: Tavadze F.N., Samsonov G.V., G.V. Tsagareishvili (eds.) Boron – Synthesis, structure and properties. Nauka: Moscow, 1974. [in Russian].

[8] C.J. Speerschneider, J.A. Sartell. Mechanical and Micromechanical Behavior of Bulk Polycrystalline Boron. In: Gaulé G.K. (eds) Boron. Springer: Boston, 1965.

[9] R.A. Andrievskii, I.A. Bairamashvili, Yu.I. Soloev, V.V. Khromonozhkin, Sintered boron – production and properties. I. Investigation of the sintering of boron, Sov. Powder Metall. Met. Ceram. 21 (1982) 622–627.

[10] R.A. Andrievskii, I.A. Bairamashvili, L.N. Dement'ev, P.V. Zubarev, A.G. Lanin, Yu.I. Soloev, M.L. Taubin, M.A. Fedotov, Sintered boron – production and properties. II. Mechanical and thermophysical properties, Sov. Powder Metall. Met. Ceram. 21 (1982) 702–705.

[11] D.R. Petrak, R.Ruh, G.R. Atkins, Mechanical Properties of Hot-Pressed Boron Suboxide and Boron, Bull. Am. Ceram. Soc. 53 (1974) 569–573.

[12] Y.G. Kim, P.A. Dowben, J.T. Spencer, Chemical vapor deposition of boron and boron nitride from decaborane(14), J. Vac. Sci. Technol. A 7 (1989) 2796–2799.

[13] Ya.A. Ugai, N.E. Soloviev, E.M. Averbakh, A.N. Parfenov, On crystallization of amorphous boron. In: Tavadze F.N., Samsonov G.V., G.V. Tsagareishvili (eds.) Boron – Synthesis, structure and properties. Nauka: Moscow, 1974. [in Russian].

[14] G.V. Tsagareishvili, F.N. Tavadze, Boron crystals – Preparation, structure and properties, Prog. Crystal Growth and Chract. 16 (1988) 341–365.

[15] D. Demirskyi, O. Vasylkiv, Consolidation and grain growth of tantalum diboride during spark plasma sintering, Ceram. Int. 42 [12] (2016) 16396–16400.

[16] D. Demirskyi, O. Vasylkiv, Analysis of the high-temperature flexural strength behavior of B4C–TaB2 eutectic composites produced by in situ spark plasma sintering, Mater. Sci. Eng. A 697 (2017) 71–78.

[17] D. Demirskyi, O. Vaslykiv, Spark plasma sintering and high-temperature strength of B6O–TaB2 ceramics, J. Eur. Ceram. Soc. 37[8] (2017) 3009–3014.

[18] D. Demirskyi, I. Solodkyi, T. Nishimura, Y. Sakka, O. Vasylkiv, High- temperature strength and plastic deformation behavior of niobium diboride consolidated by spark plasma sintering, J. Am. Ceram. Soc. 100 [11] (2017) 5295–5305.

[19] E.A. Ekimov, I.P. Zibrov, High-pressure high-temperature synthesis and structure of α-tetragonal boron, Sci. Technol. Adv. Mater. 12 (2011) 055009.

[20] E.A. Ekimov, I.P. Zibrov, A.V. Zoteev, Preparation of Boron Microcrystals via High Pressure, High Temperature Pyrolysis of Decaborane, B10H14, Inorg. Mater. 47 [11] (2011) 1194–1198.

[21] I. Solodkyi, D. Demirskyi, Y. Sakka, O. Vasylkiv, Synthesis of Multi-Layered Star-Shaped B6O Particles Using the Seed-Mediated Growth Method, J. Am. Ceram. Soc. 98 [12] (2015) 3635–3638.

[22] H. Hubert, L.A.J. Garvie, B. Devouard, P.R. Buseck, W.T. Petuskey, P.F. McMillan, High-Pressure, High-Temperature Synthesis and Characterization of Boron Suboxide (B6O), Chem. Mater. 10 [6] (1998) 1530–1537.

[23] B.F. Decker, J.S. Kasper, The crystal structure of a simple rhombohedral form of boron, Acta Cryst. 12 (1959) 503–506.

[24] J.L. Hoard, D.B. Sullenger, C.H.L. Kennard, R.E. Hughes, The structure analysis of β-rhombohedral boron, J. Solid. State Chem. 1 [2] (1970) 268–277.

[25] M.F. Garbauskas, J.S. Kasper, G.A. Slack, The incorporation of vanadium in β-rhombohedral boron as determined by single-crystal diffractometry, J. Solid. State Chem. 63 [3] (1986) 424–430.

[26] R.M. Pirzkhalaisvili, I.A. Bairamashvili, T.V. Samkurashvili, G.P. Lomidze, Sh.A. Loldze, N.I. Gudushuari, Investigation of transformation of amorphous boron into crystalline state. In: Tavadze F.N., Samsonov G.V., G.V. Tsagareishvili (eds.) Boron – Synthesis, structure and properties. Nauka: Moscow, 1974. [in Russian].

[27] R.M. German, R.W. Mar, Sintering behavior of boron, Bull. Am. Ceram. Soc., 54 (1975) 178–183.

[28] D. Demirskyi, D. Agrawal, A. Ragulya, A scaling law study of the initial stage of microwave sintering of iron spheres, Scr. Mater. 66 [6] (2012) 323–326.

[29] H.F. Rizzo, W.C. Simmons, H.O. Bielstein, The Existence and Formation of the Solid B6O, J. Electrochem. Soc. 109 [11] (1962) 1079–1082.

[30] V.L. Solozhenko, V. Bushlya, Mechanical Properties of Boron Phosphides, J. Superhard Mater. 41 (2019) 84–89.

[31] D. Demirskyi, O. Vasylkiv, Microstructure and mechanical properties of boron suboxide ceramics prepared by pressureless microwave sintering, Ceram. Int. 42 [12] (2016) 14282–14286.

[32] I. Solodkyi, D. Demirskyi, Y. Sakka, O. Vasylkiv, Hardness and toughness control of brittle boron suboxide ceramics by consolidation of star-shaped particles by spark plasma sintering, Ceram. Int. 42 [2] (2016) 3525–3530.

[33] P. Badica, H. Borodianska, S. Xie, T. Zhao, D. Demirskyi, P. Li, A.I.Y. Tok, Y. Sakka, O. Vasylkiv, Toughness control of boron carbide obtained by spark plasma sintering in nitrogen atmosphere, Ceram. Int. 40 [2] (2014) 3053–3061.

[34] D. Demirskyi, I. Solodkyi, Y. Sakka, O. Vasylkiv, High- Temperature Strength of Boron Suboxide Ceramic Consolidated by Spark Plasma Sintering, J. Am. Ceram. Soc. 99 [8] (2016) 2769–2777.

[35] M. Thiele, M. Herrmann, A. Michaelis, B6O Materials with Al2O3/Y2O3 Additives Densified by FAST/SPS and HIP, J. Eur. Ceram. Soc. 33 (2013) 2375–2390.

[36] B. Champagne, R. Angers, Mechanical Properties of Hot-Pressed B-B4C Materials, J. Am. Ceram. Soc. 62 (1979) 149–153.

[37] K. A. Schwetz, W. Grellner, The Influence of Carbon on the Microstructure and Mechanical Properties of Sintered Boron Carbide, J. Less-Com. Met. 82 (1981) 37–47.

[38] R. W. Rice, Strength/Grain-Size Effects in Ceramics, Proc. Br. Ceram. Soc. 20 (1972) 205–257.

[39] A.D. Osipov, I.T. Ostapenko, V.V. Tarosov, R.V. Tarasov, V.P. Podtykan, N.F. Kartsev, Effect of Porosity and Grain Size on the Mechanical Properties of Hot-Pressed Boron Carbide, Powder Metall. Met. Ceram. 1 (1982) 63–67.

[40] T. Vasilos, S. K. Dutta, Low Temperature Hot Pressing of Boron Carbide and Its Properties, Bull. Am. Ceram. Soc., 53 [5] (1974) 453–454.

[41] G. de With, High Temperature Fracture of Boron Carbide: Experiments and Simple Theoretical Models, J. Mater. Sci. 19 (1984) 457–466.

[42] M. Bougoin, F. Thevenot, J. Dubois, G. Fantozzi, Synthese et Caracterisation de Ceramiques Denses en Carbure de Bore, J. Less Com. Met. 114 (1985) 257–271.

[43] N.D. Rybal'chenko, A.G. Mironova, V.P. Podtykan, I.T. Ostapenko, A.D. Osipov, R.V. Tarasov, Effect of Conditions of Hot Pressing on the Structure and Mechanical Properties of Boron Carbide, Powder Metall. Met. Ceram. 8 (1983) 39–43.

[44] C.C.M. Wu, R.W. Rice, Porosity Dependence of Wear and Other Mechanical Properties on Fine-Grain A12O3 and B4C, Ceram. Eng. Sci. Proc. 6 (1985) 977–994.

[45] C.C. Seaton, S.K. Dutta, Effect of Grain Size on Crack Propagation in Thermally Shocked B4C, J. Am. Ceram. Soc. 57 [5] (1974) 228–229.

[46] N. Tamari, H. Kobayashi, T. Tanaka, I. Kondoh, S. Kose, Mechanical Properties of B4C-SiC Whisker Composite Ceramics, J. Ceram. Soc. Jpn. 98 (1990) 1159–1163.

[47] K. Hirota, Y. Nakayama, M. Kato, S. Nakane, T. Nishimura, The Study on Carbon Nanofiber (CNF)-Dispersed B4C Composites, Int. J. App. Ceram. Tech., 6 (2009) 607–616.

[48] F. Thevenot, Boron carbide – a comprehensive review, J. Eur. Ceram. Soc. 6 [4] (1990) 205–225.

[49] Th.H. Courtney. Mechanical Behavior of Materials, 2nd Edition, Waveland Press, 2005.

[50] G.V. Samsonov, Strength and plasticity of refractory compounds, Inorg. Mater. (USSR) 9 (1973) 1680–1687.

[51] Kuliiev, Ruslan, Mechanical Properties of Boron Carbide (B4C) (2020). Electronic Theses and Dissertations, 2020-. 81. https://stars.library.ucf.edu/etd2020/81.

[52] O. Vasylkiv, D. Demirskyi, H. Borodianska, Y. Sakka, P. Badica, High temperature flexural strength in monolithic boron carbide ceramic obtained from two different raw powders by spark plasma sintering, J. Ceram. Soc. Jpn. 124 (2016) 587–592.

[53] O. Vasylkiv, D. Demirskyi, P. Badica, T. Nishimura, A.I.Y. Tok, Y. Sakka, H. Borodianska, Room and high temperature flexural failure of spark plasma sintered boron carbide, Ceram. Int. 42 (2016) 7001–7013.

[54] O. Vasylkiv, D. Demirskyi, H. Borodianska, A. Kuncser, P.Badica, High-temperature strength of boron carbide with Pt grain-boundary framework in situ synthesized during spark plasma sintering, Ceram. Int. 46 [7] (2020) 9136–9144

[55] M.E. Antadze, G.V. Tsagareishvili, O.A. Tsagareishvili, D.N. Tsikaridze, A.G. Khvedelidze, Growth forms of single crystals of β-rhombohedral boron, J. Less Common Met. 117 (1986) 153–158.

[56] https://crystdb.nims.go.jp.

[57] H. Hubert, L. Garvie, P. Buseck, William T. Petuskey, P. McMillan, High-Pressure, High-Temperature Syntheses in the B-C-N-O System, J. Solid State Chem. 133 [2] (1997) 356–364.

[58] L. Garvie, H. Hubert, William T. Petuskey, P. McMillan, P. Buseck, High-Pressure, High-Temperature Syntheses in the B-C-N-O System II. Electron Energy-Loss Spectroscopy (EELS), J. Solid State Chem. 133 [2] (1997) 365–371.

[59] G.A. Slack, C.I. Hejna, M.F. Garbauskas, J.S. Kasper, The crystal structure and density of β-rhombohedral boron, J. Solid State Chem. 76 (1988) 52–63.

[60] M.E. Antadze, V.N. Rozhanskii, G.V. Tsagareishvili, F.N. Tavadze, X-ray and electron microscopic investigation of β-rhombohedral crystal of boron. In: Tavadze F.N., Samsonov G.V., Tsagareishvili G.V. (eds.) Boron – Synthesis, structure and properties. Nauka: Moscow, 1974. [in Russian].

[61] H. Werheit, Die Halbleitereigenschaften des Bors. In: Madelung O (eds) Festkörperprobleme X. Springer: Berlin, Heidelberg, 1970.

[62] H. Binnenbruck, A. Hausen, P. Runow, H. Werheit, Über Probenpräparation, Oberflächenzustand und Kristallbaufehler von einkristallinem β-rhomboedrischem Bor, Z. Naturforsch. 25 A (1970) 1431–1434.

[63] M.J. McKelvy, A.R. Rae Smith, L. Eyring, High-resolution electron microscope analysis of {100} twinning in β-rhombohedral boron, J. Solid State Chem. 44 (1982) 374–381.

[64] K. Kleinhenz, P. Runow, Herstellung dünner Bor- Folien und elektronenmikroskopische Beobachtung ihrer Baufehler, Phys. Status Solidi 29 (1968) 627–637.

[65] E. Amberger, W. Dietze, J. Jaumann, P. Runow, Preparation of α- rhombohedral boron and electron microscopic examination, Phys. Solid State A. 2 [2] (1970) K59–K61.

[66] J.P. Sitarik, W.C. Ellis, Preparation and Morphology of Boron Filamentary Crystals Grown by the Vapor- Liquid- Solid Mechanism, J. Appl. Phys. 37 (1966) 2399–2401.

[67] S. Komatsu, Y. Moriyoshi, Growth forms of β-rhombohedral boron whiskers and platelets prepared in a low-pressure B2H6 + He plasma in terms of periodic bond chain method, J. Cryst. Growth 108 (1991) 63–72

[68] R.F. Firestone, A.H. Heuer, Creep Deformation of 0° Sapphire, J. Am. Ceram. Soc. 59 [1-2] (1976) 24–29.

[69] S.M. Wiederhorn, Fracture of Sapphire, J. Am. Ceram. Soc. 52 [9] (1969) 485–491.

[70] A.G. Evans, T.G. Langdon. Structural Ceramics Pergamon Press: New York, 1976.

[71] R. Scheuplein, P. Gibbs, Surface Structure in Corundum: I, Etching of Dislocations, J. Am. Ceram. Soc. 43 [9] (1960) 458–472.

[72] A.A. Giardini, J.A. Kohn, L. Toman, and D.W. Eckart, Vector Hardness Properties of Boron and Aluminium Borides, in: Kohn J.A., Nye W.F., Gaulé G.K. (eds.) Boron Synthesis, Structure, and Properties. Springer: Boston, MA, 1960.

[73] S. Yamaoka, H. Komatsu, H. Kanda, N. Setaka, Growth of diamond with rhombic dodecahedral faces, J. Cryst. Growth 73 [3] (1977) 349–352.

[74] H. Hyodo, A. Nezu, K. Soga, K. Kimura, Self-compensation property of β-rhombohedral boron doped with high Li concentration, Solid State Sci. 14 [11-12] (2012) 1578–1583.

Figure Captions

Figure 1. SEM and X-ray diffraction of the initial boron powder. All phases belong to the #166 (R-3m) space group. The main phase was β-B rhombohedral boron with the lattice parameters (a = 10.926 Å, c = 23.809 Å, [24,25]). The minor phase had lattice parameters second phase: a = 4.858 Å, c = 12.61 Å (2.85 vol.%) [23].

Figure 2. High-resolution TEM images of the as-received boron powder indicating that boron is composed of crystals with a layered aspect (a). SAED pattern in (b) indicates the β-B phase (cif data from ref [24]). The inset of the (b) shows a diffraction simulation under the kinematical theory assumption and is in good agreement with the experimental data. Some periodic defects can be observed both within a single sheet and within a stacking of sheets. (c) shows the HRTEM details of a sheet as observed along the c-axis.

Figure 3. Isothermal densification of amorphous boron compacts using SPS.

Figure 4. Representative microstructures of boron consolidated using SPS at 1800 °. Samples were prepared by ion polishing, as regular polishing using diamond slurry caused frequent pull-out of the 10–20 μm clusters.

Figure 5. Flexural strength of boron ceramic: **(a)** variation in flexural strength of boron and boron carbide ceramics as a function of grain size [11,34–47]; **(b)** statistical variation in flexural strength at room temperature. **(c)** effect of temperature on the loading curves for bulk b15 ceramics at room temperature, at 1200 °C, and at 1400 °C.

Figure 6. Young's modulus of bulk polycrystalline boron as a function of temperature (note that there is a ±20 GPa uncertainly for every mean value). Data of Kuliev [51] for boron carbide is provided as a visual reference.

Figure 7. Fracture toughness of boron as a function of temperature.

Figure 8. Summary of high-temperature flexure experiments for boron [7], boron carbide [41,52,53], and boron suboxide [34].

Figure 9. SEM images of b15 ceramics after flexural strength tests at room temperature. White arrows indicate N-rich grains, while black arrows indicate the presence of the O-rich precipitates. Based on the TEM observations, the size of the O-rich precipitates is approximately 50–200 nm, hence the light-gray grains that are larger in size correspond to the O-rich clusters. (c) shows a macroscopic zone where the B-matrix fractures in the intergranular manner and transgranular manner. The fracture type clearly depends on the relation to the force application. The O-rich

precipitates are visible on both sides. Inset in (c) shows a macroscopic distribution of the large N-rich clusters and also illustrates the relation between the force application direction and fracture at room temperature. (d,e) shows a typical XRD pattern observed for the bulk b15 ceramic, and the blue lines indicate the Bragg position for the main phase using the same initial phase as for the powder material [24]. (e) highlighted position of peaks for the layered boron structures, while (f) provides a visual representation of the layered inclusions as seen by XRD. Such layered structures can be identified using the fracture as the N-rich phase. For these grains, multiple layers were observed following the flexural strength tests.

Figure 10. TEM images of b15 ceramics after (a) spark plasma consolidation at 1800 °C with 15-min dwell in argon and (b–d) following flexural strength tests at 1200 °C. Insets in (a, d) shows selected-area electron pattern of boron phases, identified as β-B (space group #166, using cif data from [24]). (d) shows local EDX mapping and line profile indicating the presence of the N-rich and O-rich phases in the crystalline boron matrix. (d) shows a high resolution TEM image of a portion of an area marked as 1 in (c) in the [242] zone axis. 'Stacking faults' are visible here, but these were also present in the as-consolidated material (see grains in (a)). Inset in (d) visualizes (001) planes as possible stacking faults when 242 zone axis is used.

Figure 11. Position of B20 atoms with low partial occupancy in the β-boron according to structure refinement in [59]. (b) highlights the (100) plane for rhombohedral β-boron.

Figure 12. SEM micrographs of boron-15 after flexural tests at ambient temperature (a-d), at 1200 °C, and at 1400 °C (e,f). (a,b) were taken in the area at the ~40° angle to the load application direction, while (c-f) were taken from the surface perpendicular to the load application direction (top to bottom). The white arrows in (b,d) show places of quasi-brittle fracture previously reported for boron suboxide [31,34], and are the result of the fracture along (012) rhombohedral plane. The black arrow in (f) shows high-temperature plastic (rubberlike) deformation of layered boron grains (see higher magnification in (h)). (g) shows oversimplified view of (e) underlining the continuous nature of the matrix (blue (32 vol.%)) and suggesting that 2/3 of the grains fractured alongside the low-temperature mechanism (see **Figure 14(c**), while with an increase in temperature to 1400 °C, this value decreases below 10 vol% as the high-temperature slip-system should be dominant.

Figure 13. SEM images of b15 ceramics after flexural strength tests at 1200 °C. (a) shows an icosahedron which consists of 20 individual tetrahedral (which is the structure commonly observed for boron suboxide after high-pressure synthesis); right image illustrates relationship between

icosahedron and rhombohedral cell. (b) shows the relationship of the rhombohedral cell of β-B and its hexagonal representation. The green plane selected in the β-B cell is (012) using the hexagonal indexes; the rhombohedral sapphire experiences conchoidal surfaces when fractured along this plane [68–71]. (c) Shows the (012) plane for the **Figure 12 (b)**, where the formation of conchoidal surfaces is highlighted in red. The blue highlights the typical fracture along the prismatic plane (presumably (100)). Formation of the pentagonal-shaped structures was also seldomly observed along the icosahedron faces. Inset in (c) provides an oversimplified illustration for the relation between the basal plane (001) and (012) lamellae form during growth of the rhombohedral crystals. The black arrows in (c) and (d) indicate the presence of nitrogen-rich phases.

Figure 14. SEM images of b15 ceramics after flexural strength tests at 1200 °C, where the white arrows shows orientation of boron grains with the respect to the force application direction. Similar fracture has been reported for boron suboxide below 1000 °C in [34] and after consolidation in [31]. In principle, if grains consist of layered sub-grains, this fracture mechanism should not be limited to boron-rich compounds. (b) depicts a nominal fracture mechanism of quasi-transgranular fracture, as decohesion is assumed to be active for a boron ceramic at elevated temperatures. Directions for fracture in (a) were determined by OrientationJ (ImageJ), and note that the conchoidal surfaces usually form along the (012) plane. (c and d) provide a schematic comparison of two slip systems previously observed by Scheuplein [71]. (c) is typical for low temperature deformation, while (d) corresponds to the high-temperature slip system.

Dear Editor of Materialia, Professor Sylvain Deville,

We would like to submit the revised version of the manuscript entitled “Fracture peculiarities and high-temperature strength of bulk polycrystalline boron” by Dmytro Demirskyi, Petre Badica, Andrei Kuncser and Oleg Vasylkiv for publication in Materialia.

First, the authors would like to express our gratitude to you, and reviewers, as the feedback we received during review process helped us to correct some of the issues obtained during our work writing this manuscript.

In the revised manuscript, changes were highlighted using a yellow background color.

In order to address comments raised by the reviewer we added SEM figure (now figure 4, and corrected/altered the related discussion.

As suggested, we rewrote the abstract, conclusions, and the introduction of the manuscript.

The concise replies to the reviewers comments are provided below.

Reviewer #2: I will suggest the authors to include a paragraph where it will be explained in detail why it is important to conduct such research. In other words, it is necessary to improve the contextualization of this manuscript.

Finally, the abstract as well as the conclusions of this manuscript should be re-writed in order to make them understandable.

Thank you, we revised these sections of the manuscript.

Reviewer #3:

1) SEM images are provided for starting powders as well as for fracture surfaces, but no images are shown for as sintered materials. It would be nice to include one for the reader to see the grain structure and size, and the authors should have plenty available as they needed them to determine average grain size.

We introduced the **Figure 4** in order to present the typical grain sizes that can be detected by the SEM. We can provide a histogram for the grain-size measurement if needed. The SEM presented here is for the boron polished using ion-milling.

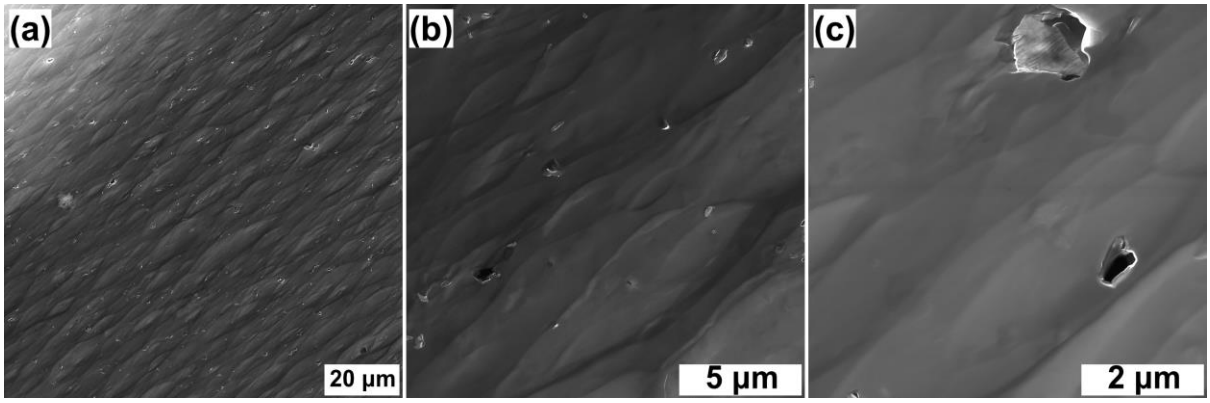

2) On the matter of grain size in the as sintered specimens at 1800 ºC, authors simply quote a grain size below 2 um, but inf Fig. 4a, the data point from this paper is at roughly ~0.9 um, so the authors must have determined this value. Please give the actual grain size, along with its standard deviation, in the manuscript.

Thank you. We update the manuscript. We show both the average grain size, and the median value.

3) Judging by the shape of stress-strain curves in Fig. 4c, the linear range is limited and the slope is thus difficult to determine precisely. This casts some doubts on the elastic moduli measurements. Authors should give more detail as to how they determined the Young's moduli. During bending experiments, were displacements measured directly at the sample using a strain gauge or LVDT or is it simply the travel of the testing machine's crosshead? Was the compliance from the frame and fixtures taken into account? Please add error bars in Fig. 5 instead of simply quoting the standard deviation in the caption.

Thank you. We updated the figure. We want to add that the Shimazu software used on the setup instantly correct (accounts) for the thermal expansion of the frame, fixtures and the crosshead movement, thus the ‘initial’ value we use to determine the Young’s moduli may contain numerical error c. For simplicity, we will provide the error obtained between the specimens tested at the same temperature.

4) Weibull analysis was shown in Figure 4b for the RT tests. Do authors have enough data to perform similar analysis for the high-temperature strength?

Possible, but results cannot be interpreted correctly because of the number of points. The example for 1000°C is provided below. Both the m and R^2 are were calculated automatically. Authors seen some strange examples of Weibull plots for 3 or 4 points in the peer-review articles, but from the viewpoint of statistics we see the lowest number of experiments of at least 12. (For RT here one can see the 10 points, we used 12 for analysis, as two of the values were identical to the error of 0.1 MPa.)

If necessary, we can implement such a graph in the manuscript, but we honestly think that for this case the mean/average value with a deviation is more appropriate.

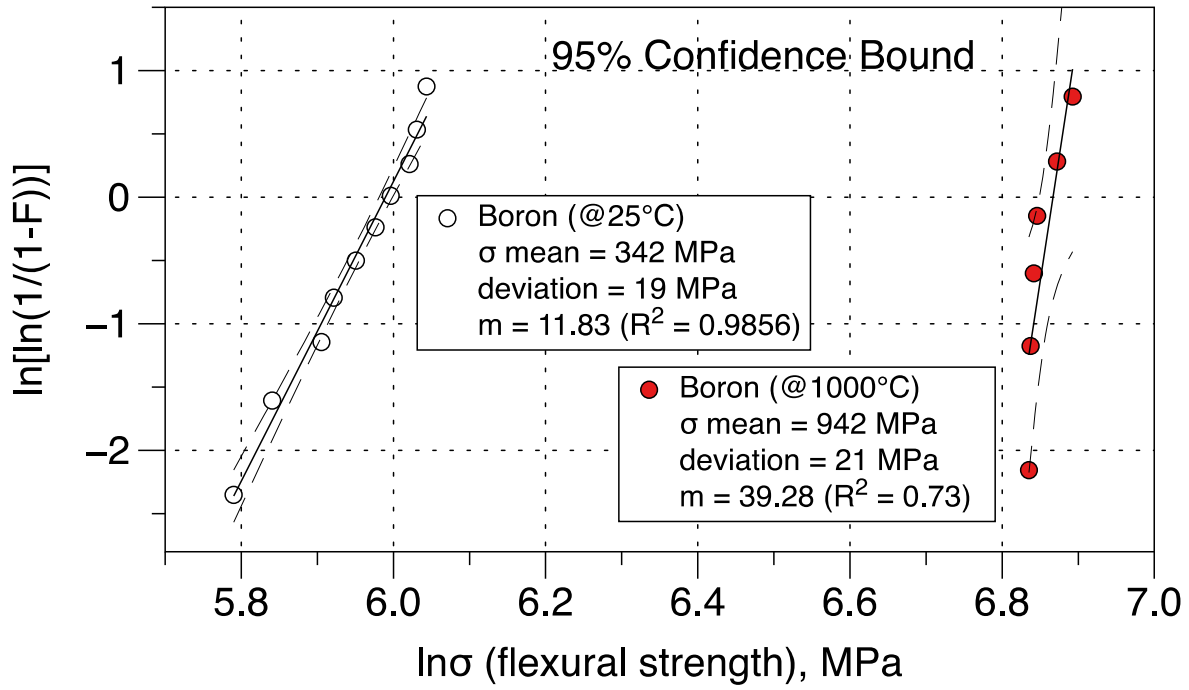

5) In Figure 2 some periodic defects are observed. Are the authors sure that these are actual defects and not Moiré fringes due to overlapping sheets with different orientations?

We thank reviewer for important observation. The investigated material is composed out of well crystallized thin sheets, as observed in the HRTEM images. If two sheets with different orientations overlap, Moire fringes should appear, indeed.

a) Figure 2 area 1: Provided the uniform mass-thickness contrast, the existence of overlapping additional B-sheets is unlikely; Hence we observe defects.
b) Regarding the upper left area of Figure 2, there is an obvious overlap of at least two B sheets. If the overlapping resulted in the generation of Moire Fringes, they should have been present in the whole overlapping area. Therefore in this area it is difficult to decide on the defects presence with high certainty.

6) In the caption of Figure 9, please check the sentence "The 'stacking faults' shown here correspond to lamellae of twinned ceramic between larger in size two stacking faults." for clarity.

Sorry we forgot to delete this sentence: “The ‘stacking faults’ shown here correspond to lamellae of twinned ceramic between larger in size two stacking faults”.

7) At the beginning of page 18, please check the meaning of "C was present as the 0.2 carbon atom in the hexagonal unit cell of β-boron which contains ~320 boron atoms". Do you mean that there are 0.2 carbon atoms on average in the unit cell, out of 320 possible sites?

Thank you. We corrected this sentence as:

At the same time, the authors of the ref. [59] suggested that the dominant impurity was carbon (150 ppm). However, the analysis in [59] suggested that 2 carbon atoms should be present in the 10 hexagonal unit cells of β-boron (each contains ~320 boron atoms).

8) Later in the paragraph we read that "Phases rich in oxygen and nitrogen were clearly observed by the SEM after the flexural tests at room temperature and by the TEM during analysis of specimens after the flexural tests at room or at elevated temperatures." Some TEM images are included in Figure 9, but please include some SEM images as well.

We modified the sentence as follows: "Phases rich in oxygen and nitrogen were clearly observed by the TEM during analysis of specimens after the flexural tests at room and at elevated temperatures."
As for the SEM, we provided our interpretation for these phases in **Fig 8** (now **Fig. 9**) for the specimens fractured at RT. At higher temperatures, we could not precisely identify the oxygen-rich phase, as we state later in the draft.
Hopefully the revised copy of this manuscript will look more satisfactory to the reviewer and to the future reader.

All authors have seen and approved the manuscript for submission to Materialia.
On behalf of authors,
Dmytro Demirskyi

Figure 1

Click here to access/download;Figure;figure1.tiff

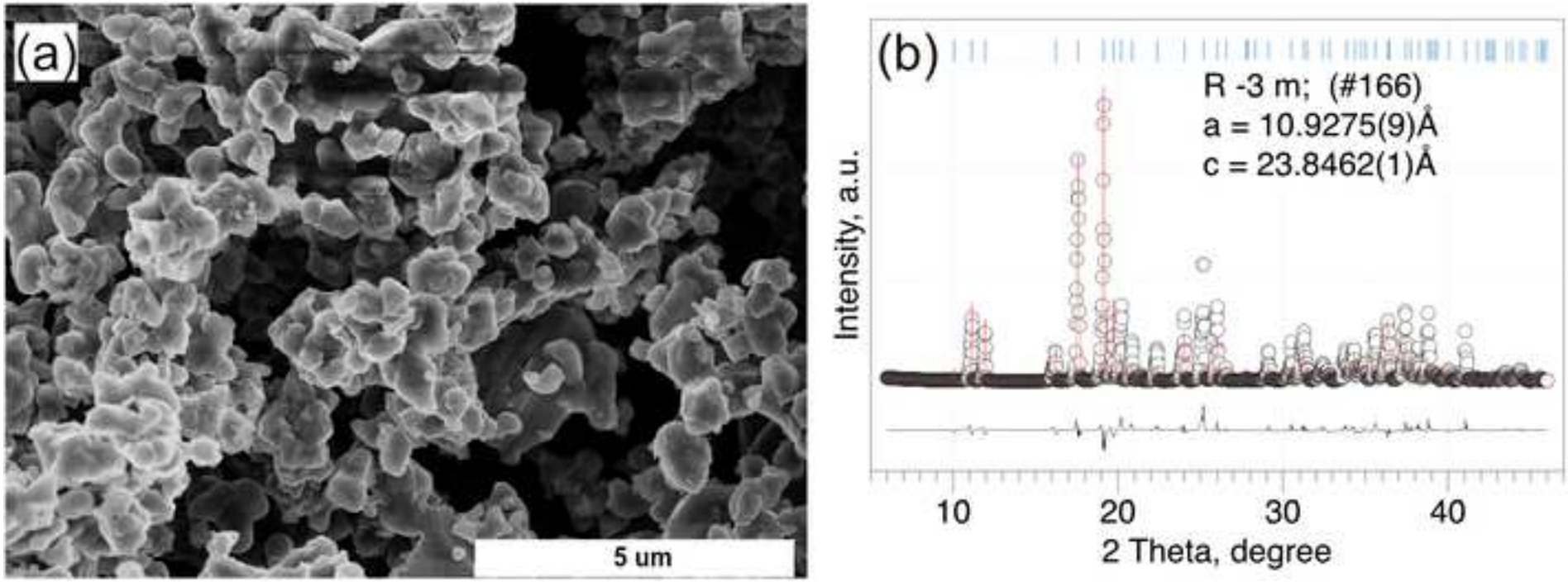

Figure 2

Click here to access/download;Figure;figure2.tiff

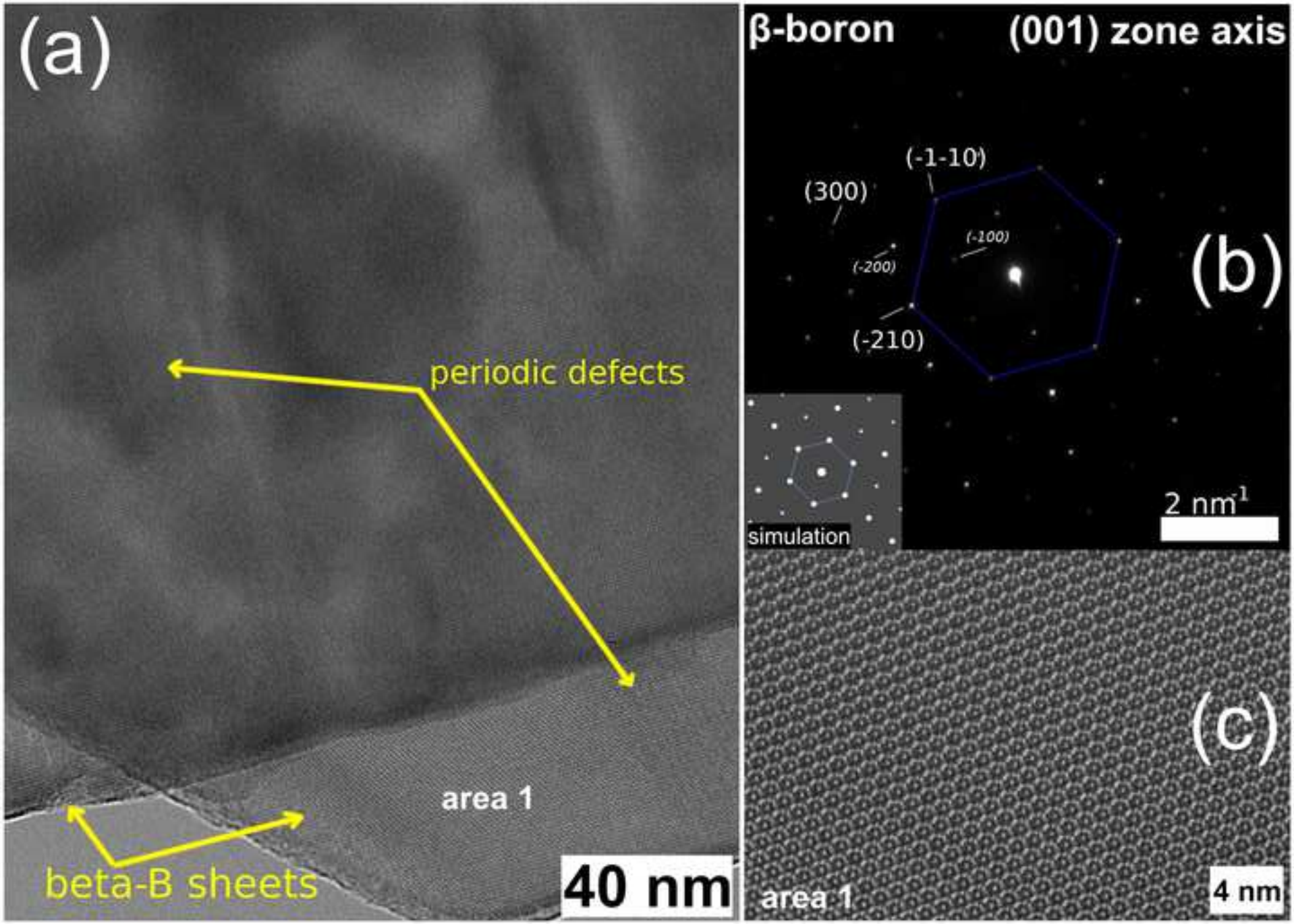

Figure 3

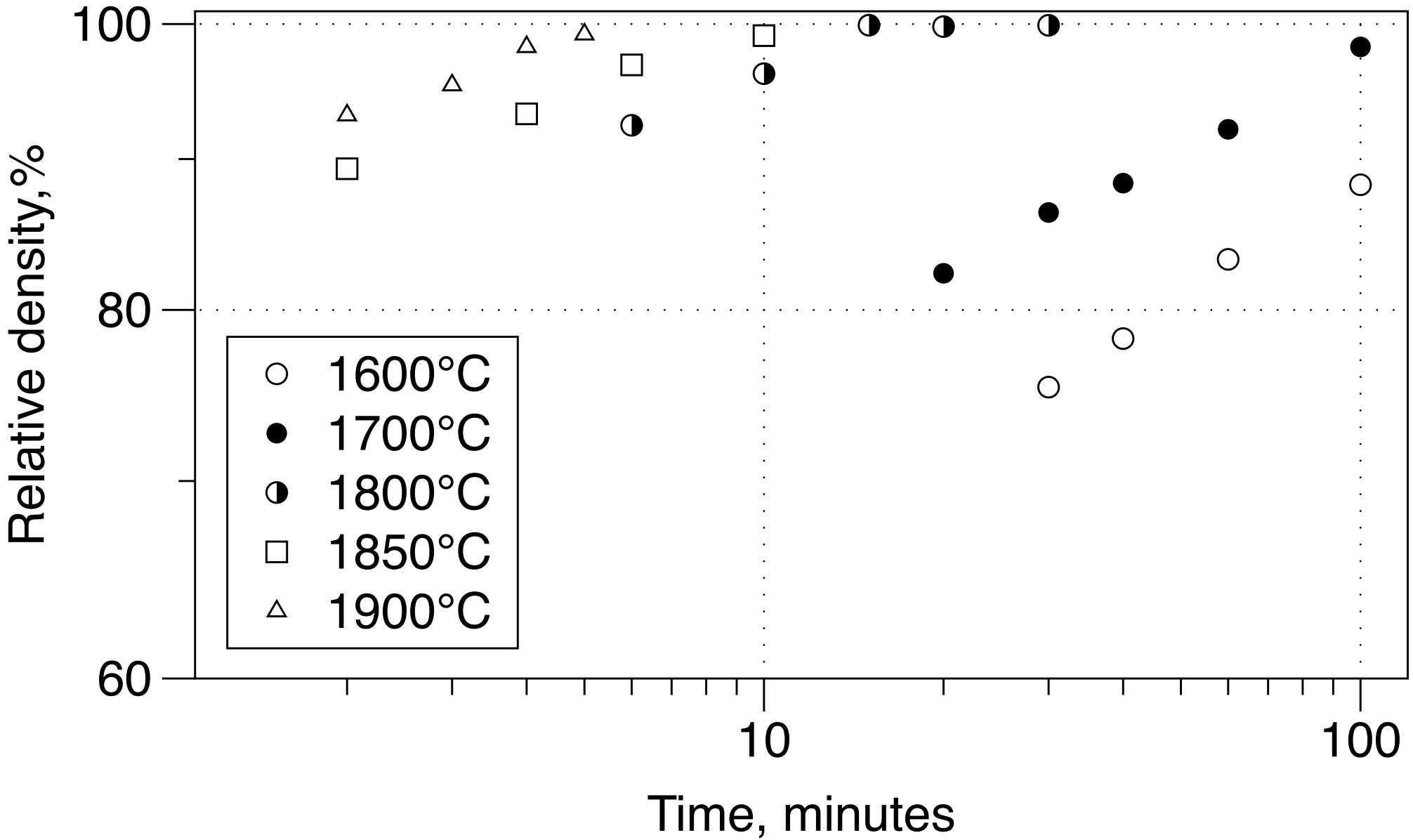

Figure 4

Click here to access/download;Figure;figure4r1.tiff

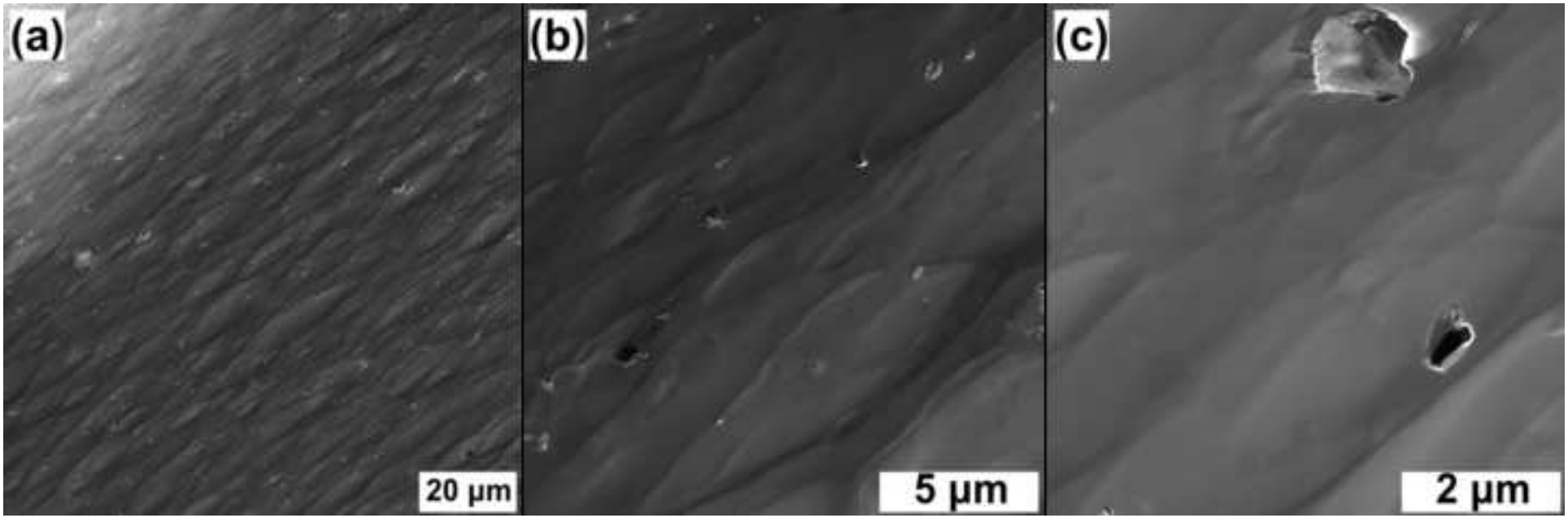

Figure 5

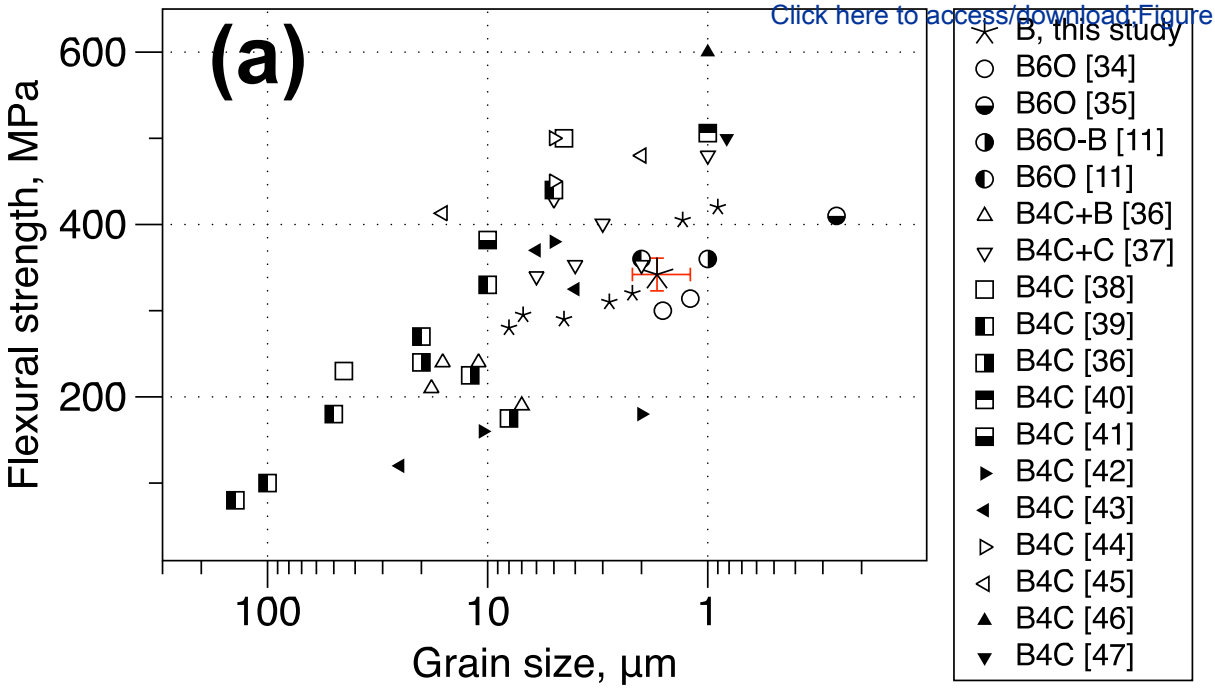

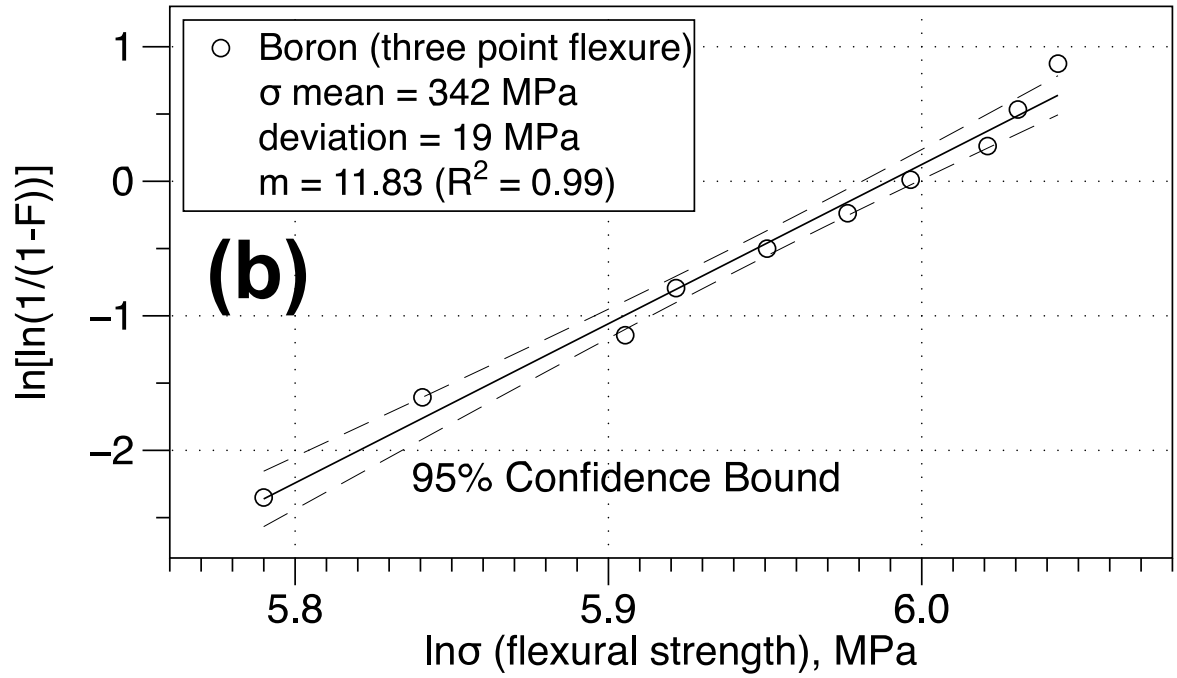

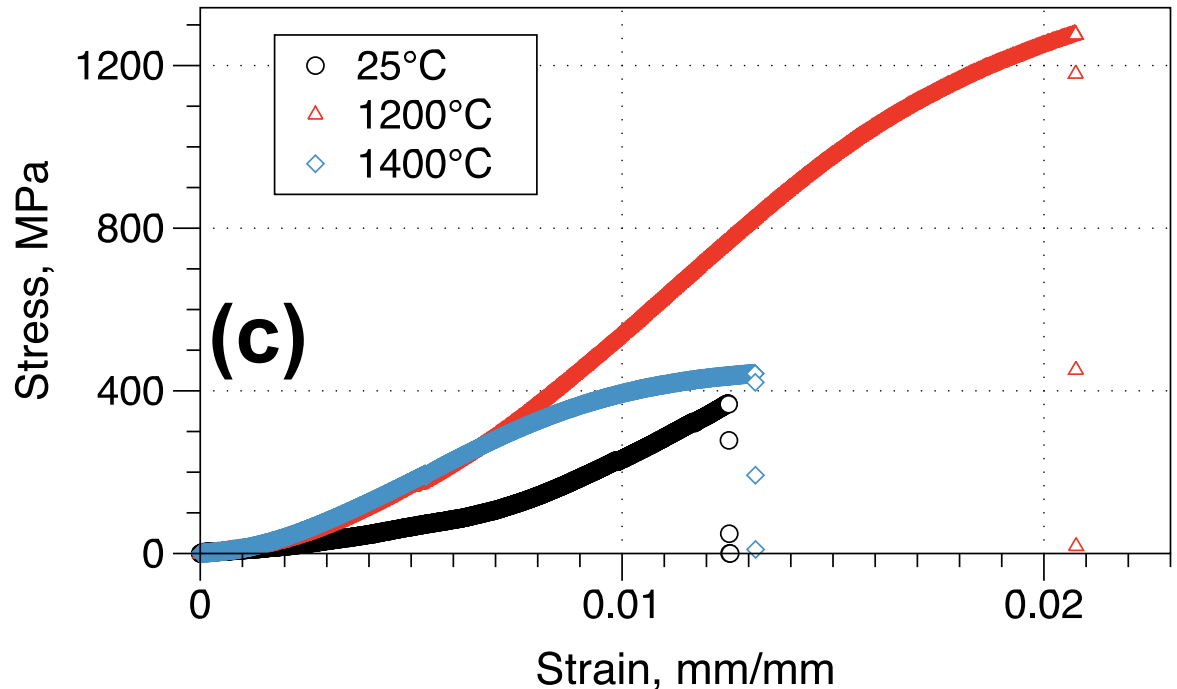

Figure 6

Click here to access/download;Figure;figure6r1.eps

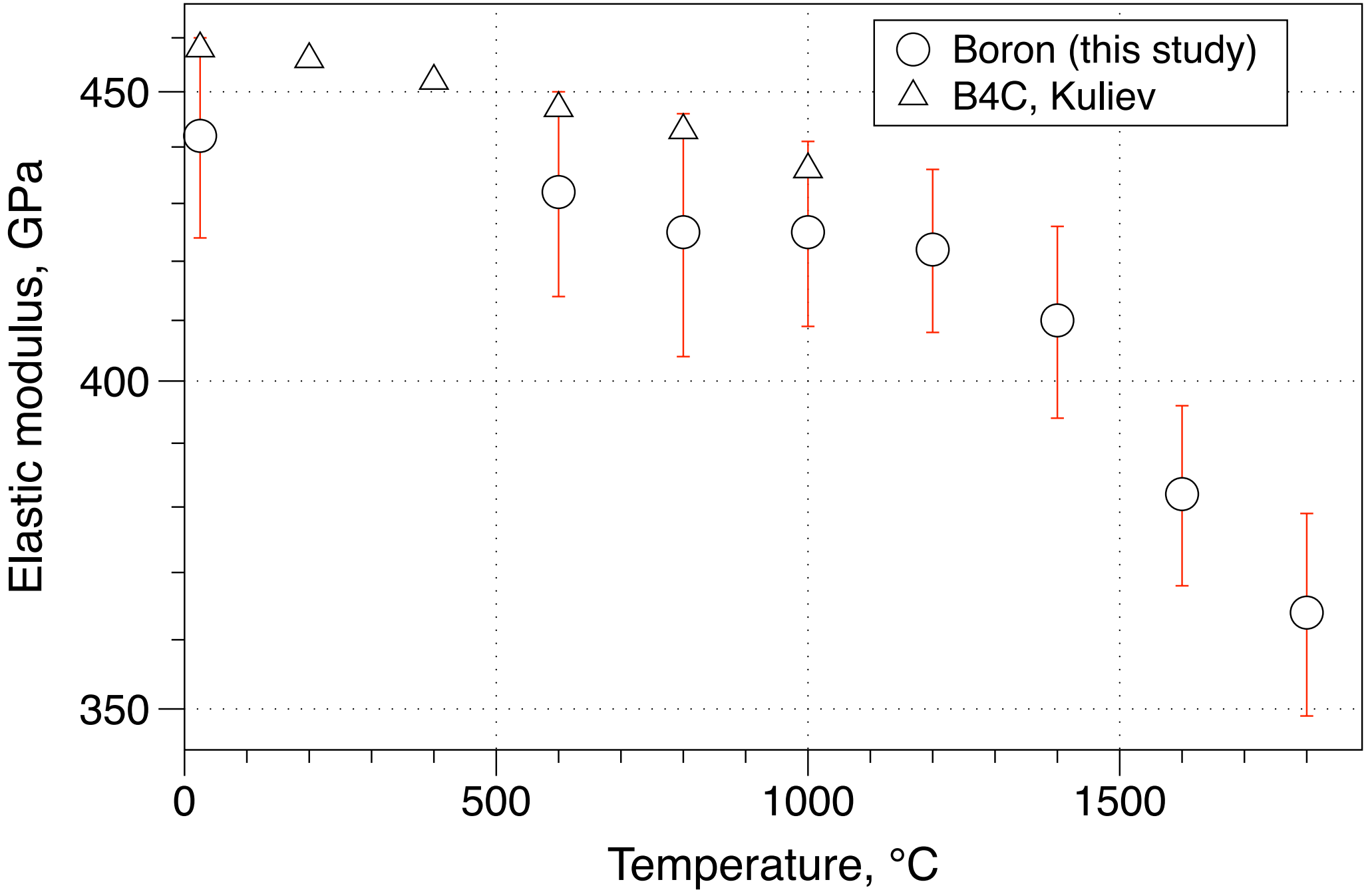

Figure 7

Click here to access/download;Figure;figure7r1.eps

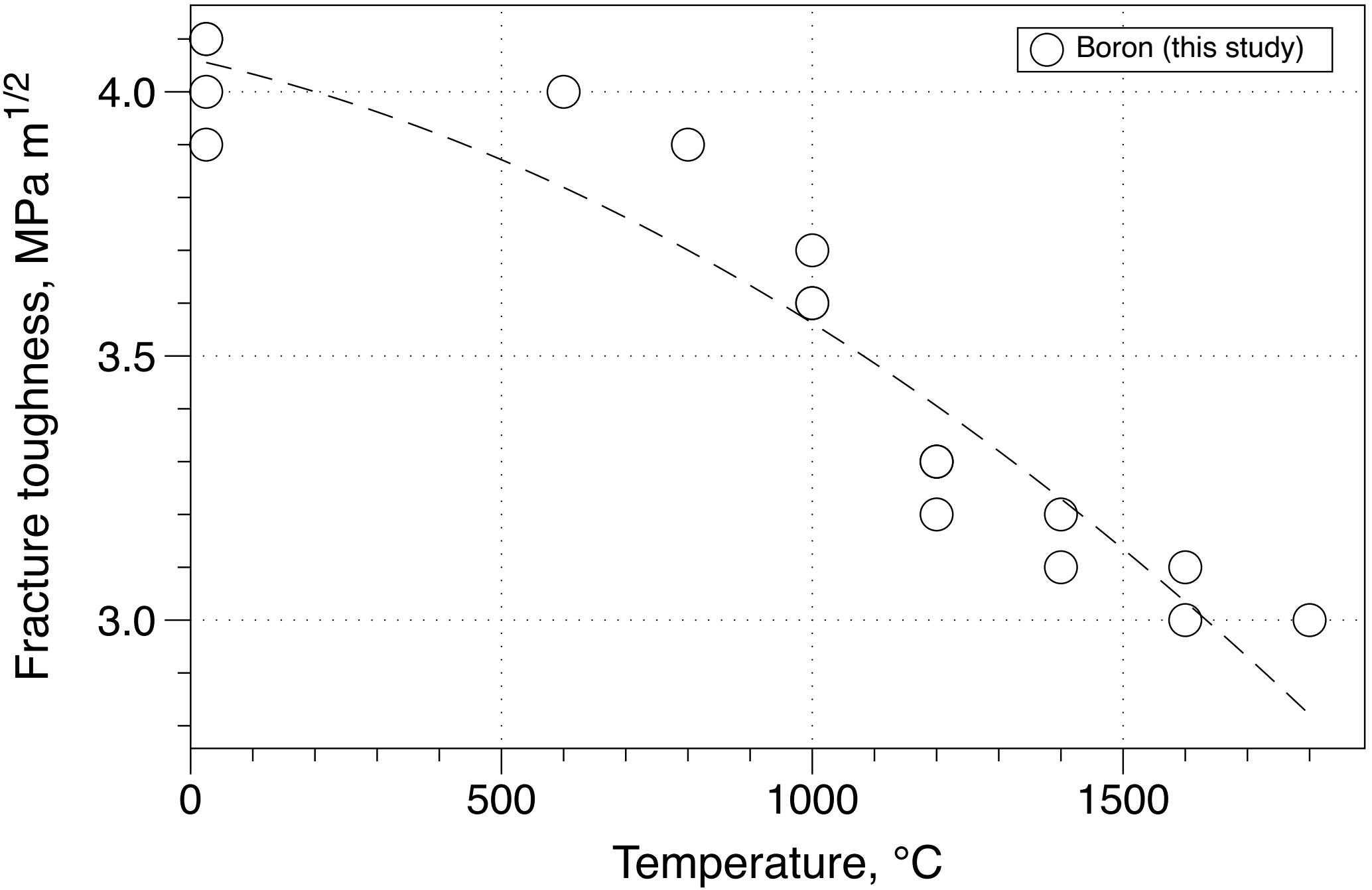

Figure 8

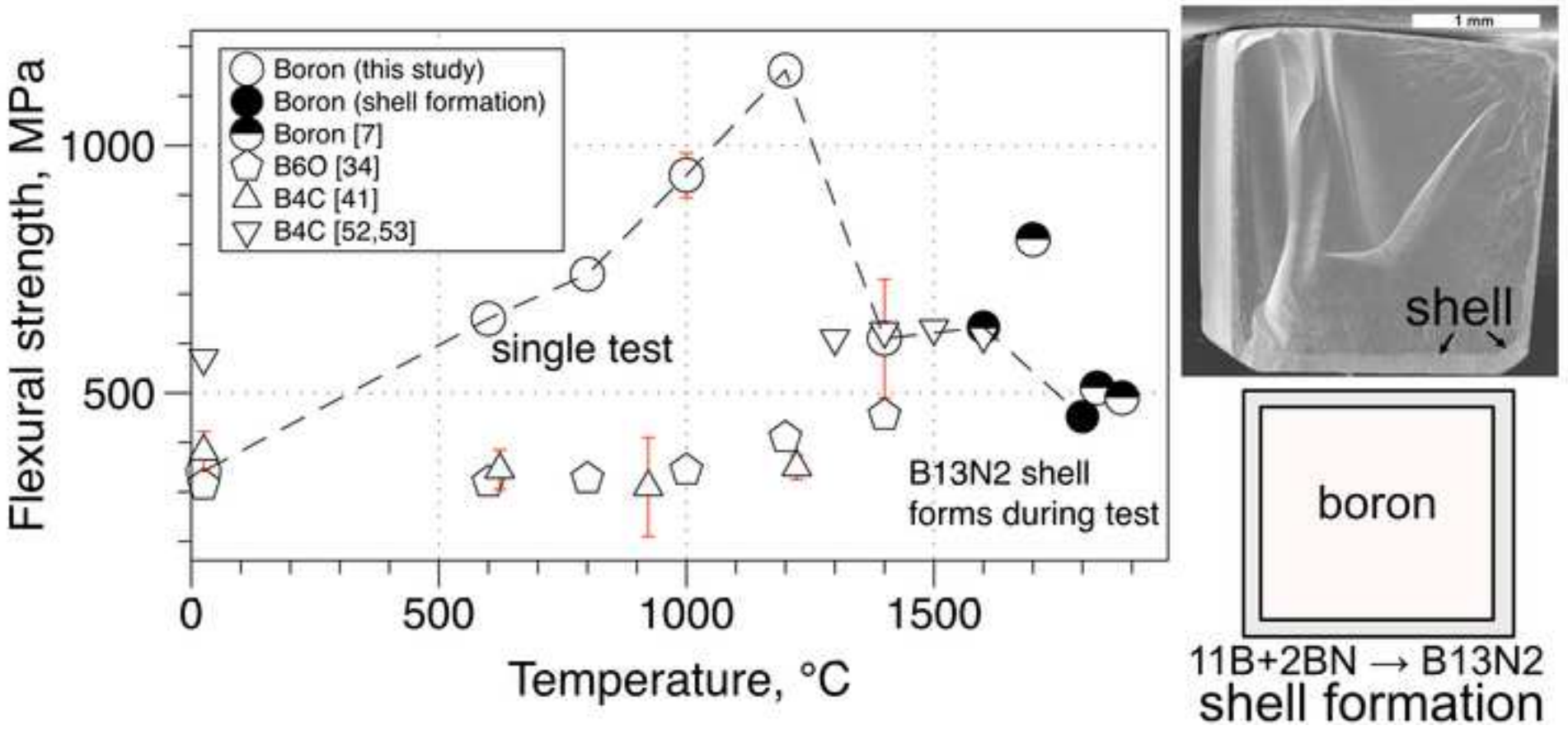

Figure 9

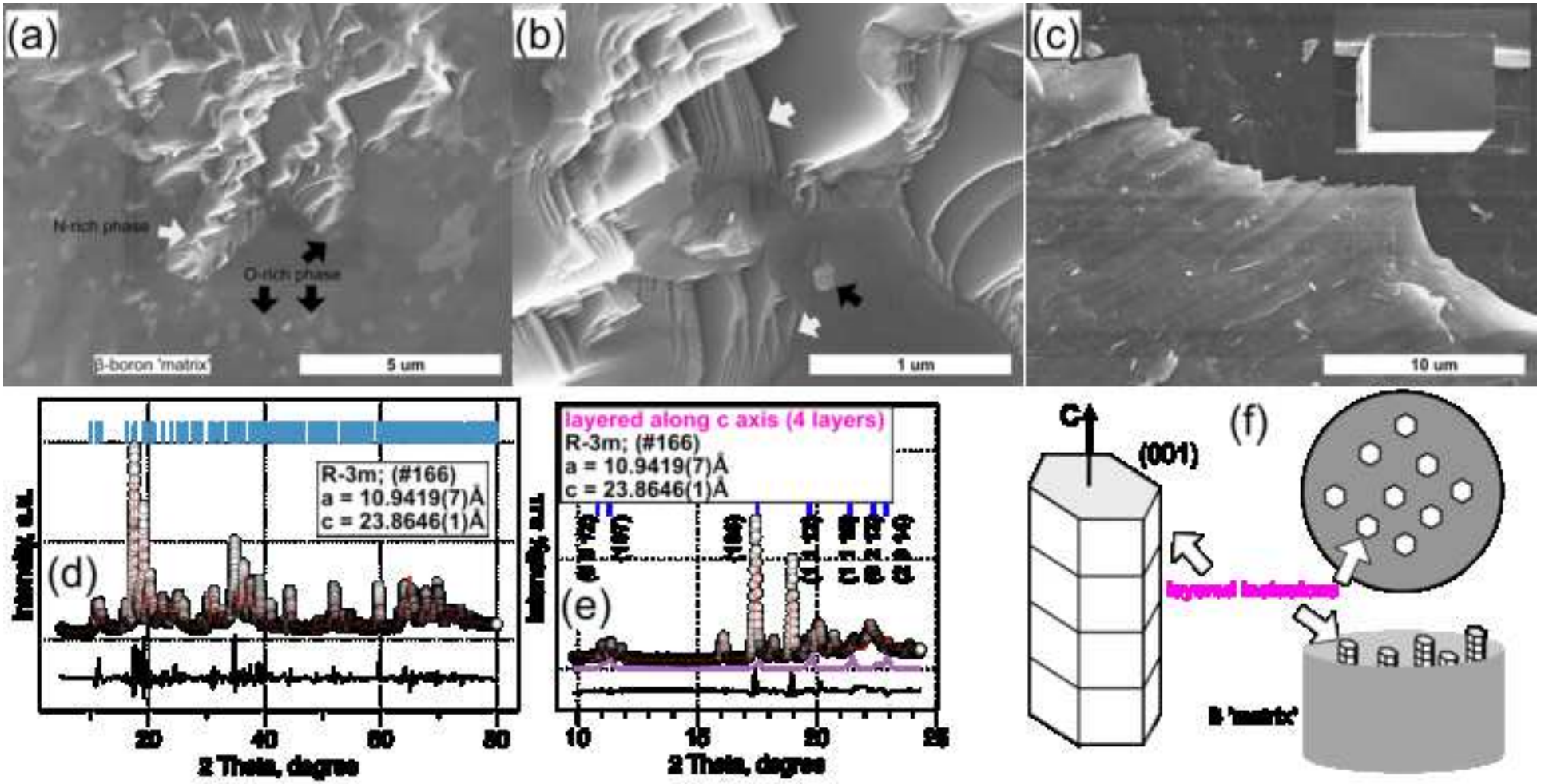

Figure 10

Click here to access/download;Figure;figure10r1.tiff

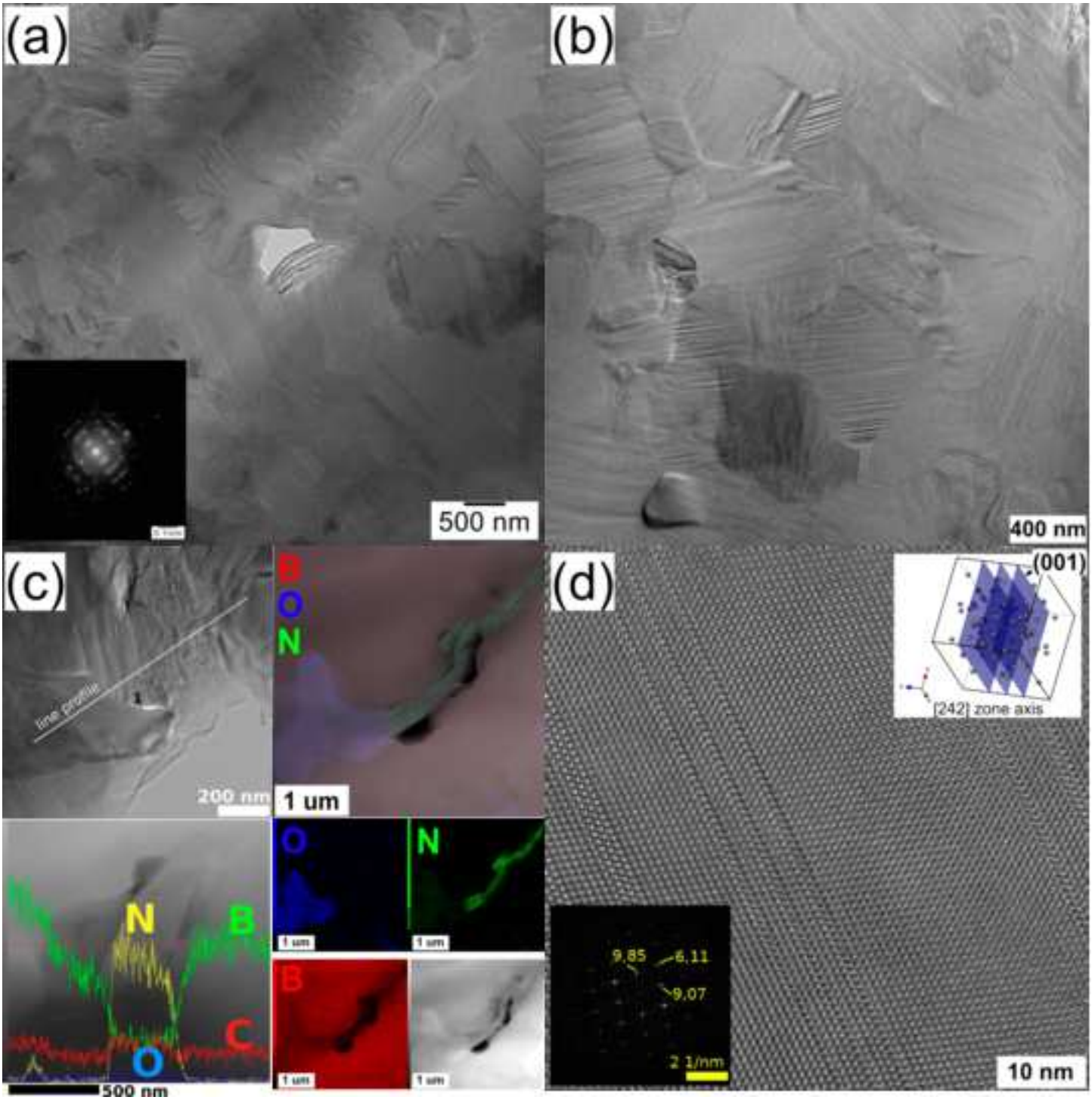

Figure 11

Click here to access/download;Figure;figure11r1.eps

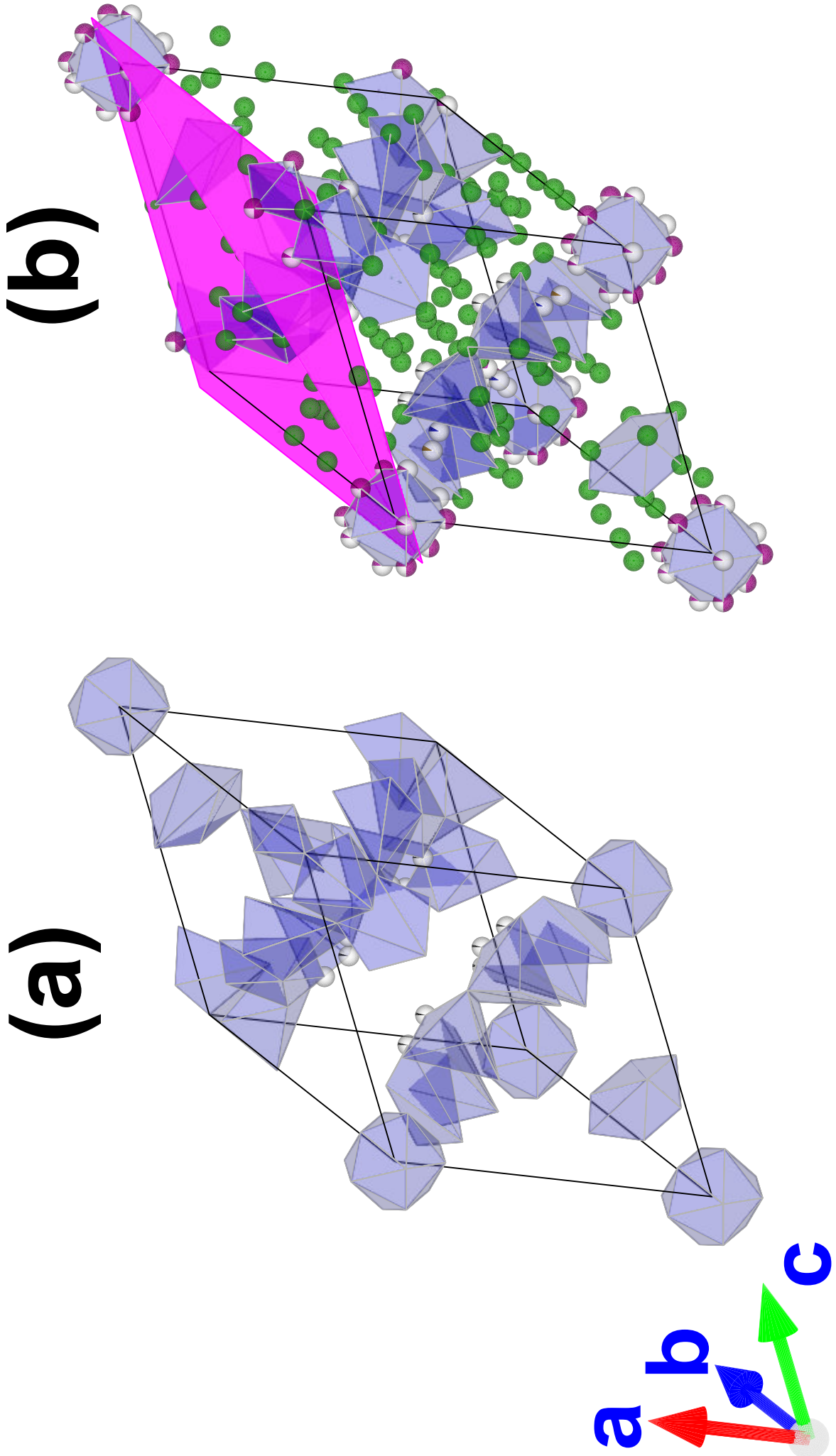

Figure 12

Click here to access/download;Figure;figure12r1.tiff

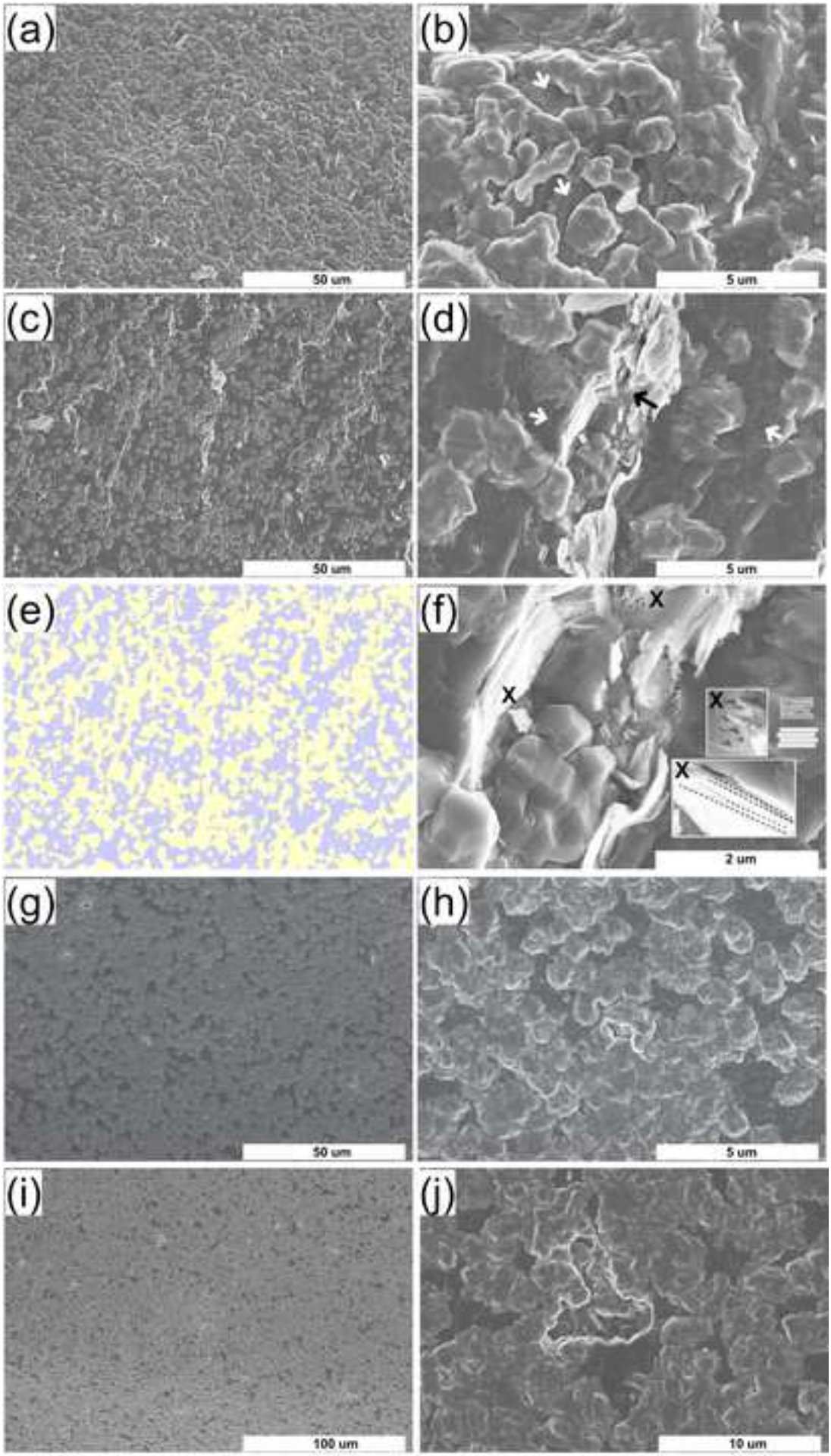

Figure 13

Click here to access/download;Figure;figure13r1.tiff

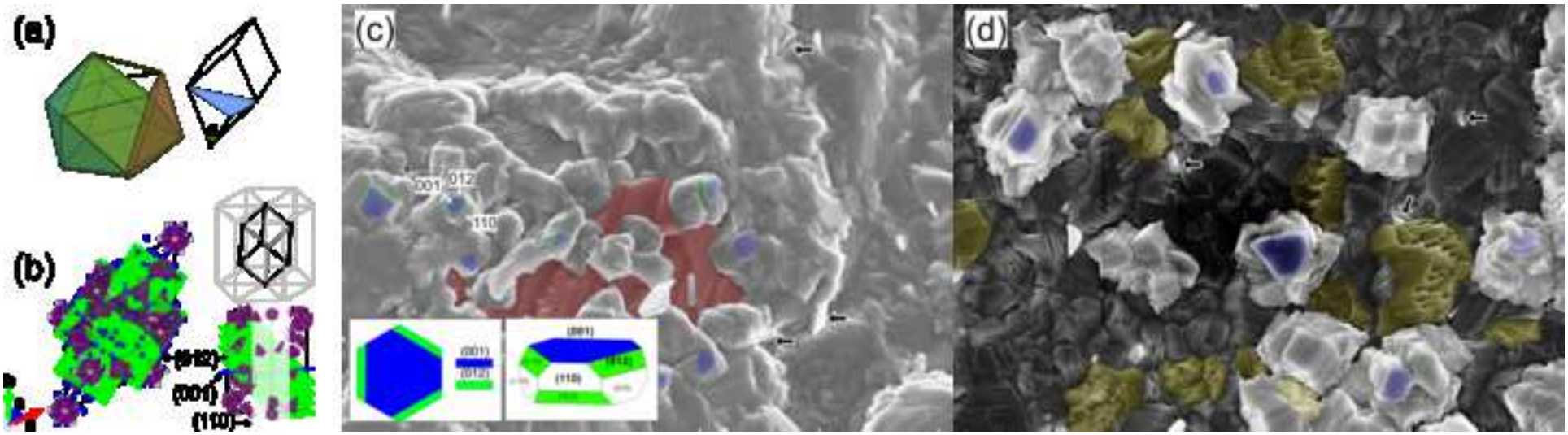

Figure 14

Click here to access/download;Figure;figure14r1.tiff

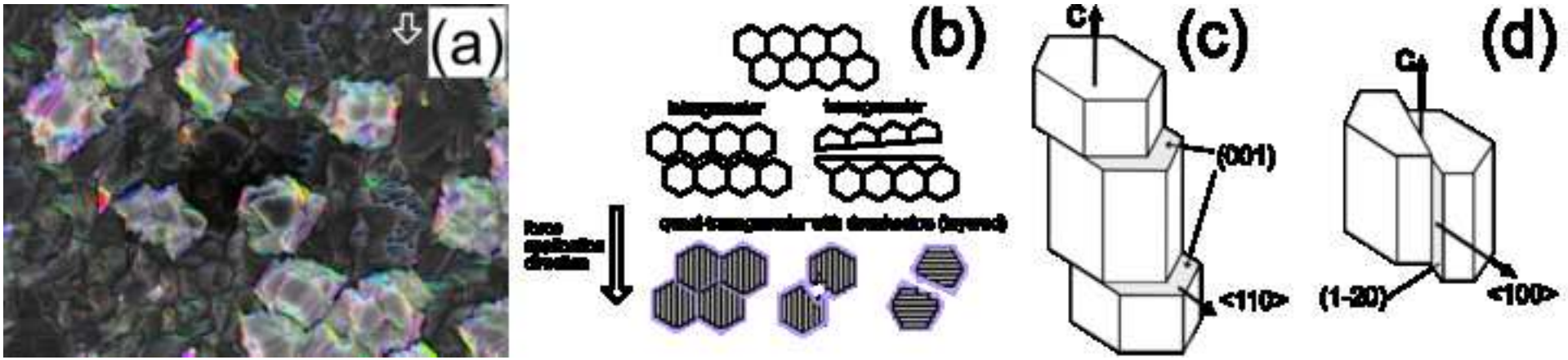

High-temperature strength and fracture of boron

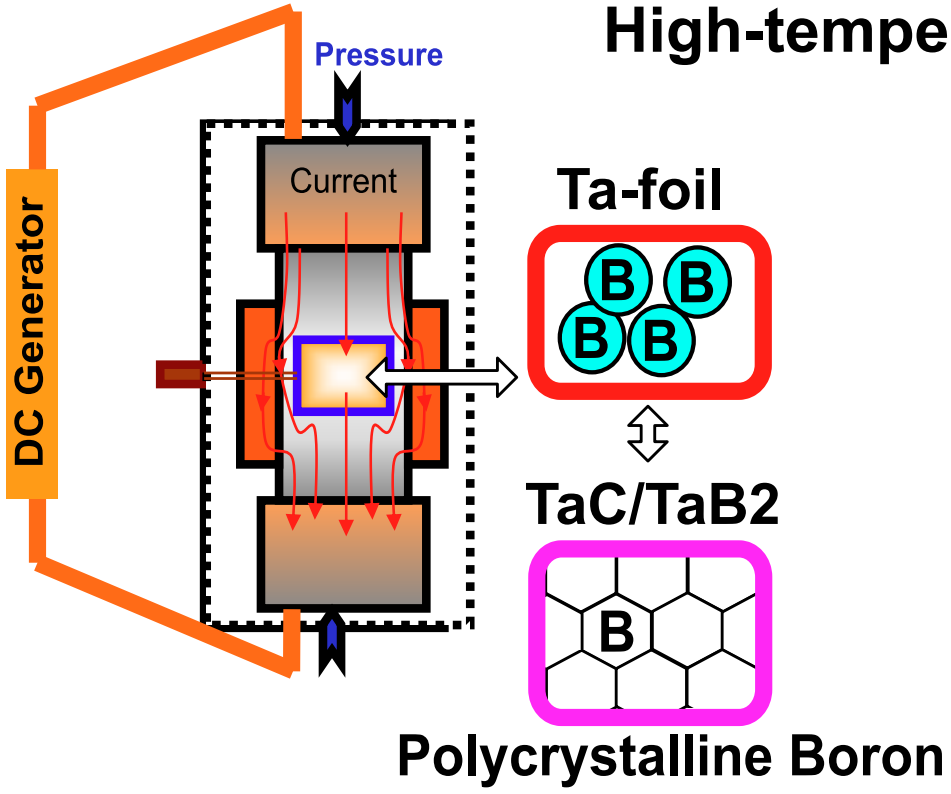

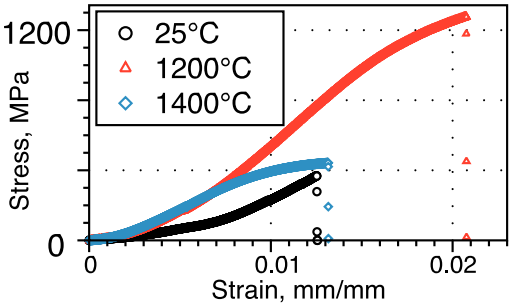

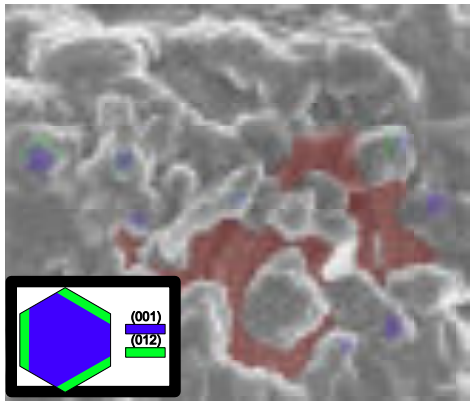

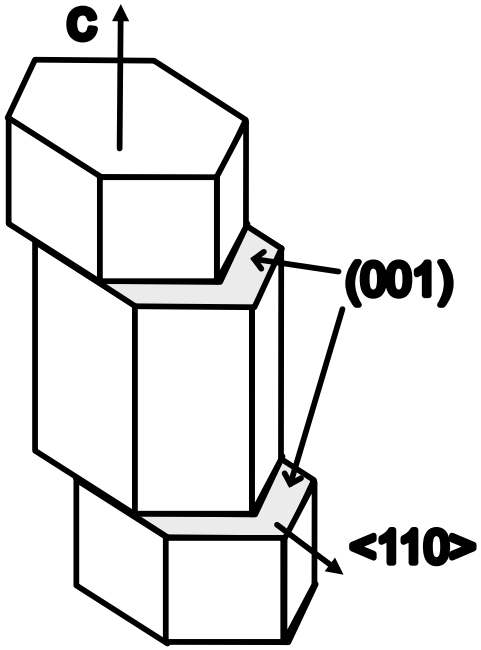

Declaration of interests

☒ The authors declare that they have no known competing financial interests or personal relationships that could have appeared to influence the work reported in this paper.

☐The authors declare the following financial interests/personal relationships which may be considered as potential competing interests: